Christine Luz Antunes

Licenciada em Ciências da Engenharia Química e Bioquímica

Adsorbent Particle Design for Application in Gas Adsorption Processes

Dissertação para obtenção do Grau de Mestre em

Engenharia Química e Bioquímica

Orientadora: Isabel A.A.C. Esteves, Investigadora Auxiliar, FCT/UNL, LAQV-Requimte

Co-orientadores: Rui P.P.L. Ribeiro, Investigador Pós-Doutoramento, FCT/UNL, LAQV-Requimte

José P.B. Mota, Professor Catedrático, FCT/UNL, LAQV-Requimte

Júri

Presidente: Mário F.J. Eusébio
Arguente: Ricardo J.S. Silva
Vogal: Isabel A.A.C. Esteves

FACULDADE DE CIÊNCIAS E TECNOLOGIA
UNIVERSIDADE NOVA DE LISBOA

March, 2016

Adsorbent Particle Design
for Application in Gas Adsorption Processes

Este documento foi gerado utilizando o processador (pdf)LaTeX, com base no template "unlthesis" [1] desenvolvido no Dep. Informática da FCT-NOVA [2].
[1] https://github.com/joaomlourenco/unlthesis [2] http://www.di.fct.unl.pt

Aos meus pais.

Acknowledgements

Quero agradecer à Professora Dr.ª Isabel Esteves e ao Dr. Rui Ribeiro por todo o apoio e orientação que me deram ao longo de todo este processo. Durante estes últimos seis meses a realizar esta dissertação mostraram-se sempre disponíveis e deram-me um apoio único ao ensinar-me e a motivar-me para desenvolver da melhor forma este trabalho. Também gostaria de agradecer ao Professor Dr. José Mota pelo o seu apoio e motivação que sempre me demonstrou ao longo do curso e durante a realização deste trabalho.

Um agradecimento especial à Aiala Garate que trabalhou e colaborou comigo e especialmente pela sua amizade.

Tenho também que agradecer à Faculdade de Ciências e Tecnologias da Universidade Nova de Lisboa por me ter proporcionado as melhores condições de ensino e de trabalho nos últimos anos.

Aos meus pais, por acreditarem em mim desde de sempre, por me motivarem e me terem ajudado a ser a pessoa que sou hoje. Sem eles não estaria neste momento a concretizar um dos meus maiores desafios. A toda a minha família e em particular à minha irmã Laurie, por me terem apoiado sempre.

A ti Luis Reis, tiveste sempre ao meu lado nestes últimos anos e tens sido o meu pilar. Obrigado pela tua paciência e por todo o teu amor.

Aos meus amigos Rui Silva e Miguel Saraiva, que tiverem comigo desde do primeiro dia na FCT. Às minhas amigas do coração Cristiana Maia e Inês Antunes pela amizade única ao longo de 20 anos. Ao Pedro Amaral e Mauro Soares por todos os momentos que vivemos juntos nos últimos anos. Às novas amizades criadas Gabriela Cardoso e Joana Santos, por tornarem os meus dias na FCT mais divertidos e noites no VII mais toleráveis.

Abstract

Metal-organic frameworks (MOFs) are novel materials that are showing great potential for different applications and in particular for gas adsorption-based separation processes. MOFs have been subject to a growing scientific interest due to their particular framework versatility and also because they have higher porosity and surface areas in comparison to other traditional adsorbents. Since these materials are relatively new, they are still only mostly studied in their primary powder form. To further study the feasibility of application of MOFs in gas adsorption processes such as Pressure Swing Adsorption (PSA), these must be shaped into body like forms, such as pellets or extrudates.

One particular MOF, aluminum terephthalate (MIL-53(Al)) has a very high surface area with a great capacity to adsorb a large amount of gases such as carbon dioxide (CO_2). Due to its characteristics there is interest in further studying this material in gas adsorption processes. Therefore, the objective of this work is to shape MIL-53(Al) with different techniques and study the characteristics of the formulated particles.

MIL-53(Al) was shaped using two different methods: compression without a binder (binderless) and extrusion with a binder. The binderless method resulted in two samples, one with a 1ton-force compression and another with a 0.5ton-force compression. Polyvinyl alcohol (PVA) was used as a binder to shape four samples with percentages of binder between 2% and 15%. The obtained shaped materials were characterized using several mechanical, structural and physico-chemical techniques. Furthermore, CO_2 adsorption equilibria measurements were performed to understand the adsorption capacity of shaped MIL-53(Al) and compared it to its primary powder form. The shaped materials with the best characteristics to be used in CO_2 gas adsorption processes were the binderless sample of 0.5ton-force compression and the sample with 5% of PVA binder. Overall, both methods show good potential in shaping MIL-53(Al) and may be a good fit for future scale-up studies.

Keywords: Gas Adsorption Equilibria, Adsorbent Materials, Metal-organic frameworks (MOFs), Carbon Dioxide CO_2, Adsorbent Shaping Design.

Resumo

Os adsorventes orgâno-metálicos, mais conhecidos como *Metal-organic frameworks* (MOFs) em terminologia inglesa, são materiais recentes que têm vindo a demonstrar grande potencial para diferentes aplicações, em particular para processos de separação e purificação por adsorção gasosa. Os MOFs têm sido alvo de um crescente interesse pela comunidade cientifica devido às suas características particulares, possuindo uma estrutura flexível, adaptável à aplicação desejada e também elevadas porosidades e área superficial, quando comparadas com outros adsorventes tradicionais. Em geral, os MOFs são produzidos em pó, sendo maioritariamente estudados nesta forma. No entanto, para estes materiais serem aplicados em processos de separação de gases, como o comum em *Pressure Swing Adsorption* (PSA) em terminologia inglesa, têm que ser moldados numa forma mais compacta de maior dimensão, seja sob a forma de grânulos, esferas ou peletes cilíndricas, habitualmente por via da compressão ou extrusão.

Um MOF em particular, o tereftalato de alumínio MIL-53(Al), tem uma área superficial e uma capacidade grandes para adsorver quantidades significativas de gases como o dióxido de carbono (CO_2). Assim, devido às suas características, existe interesse em estudar este material em processos de adsorção gasosa. Portanto, chega-se ao objectivo principal deste trabalho, onde se pretende dar forma ao MIL-53(Al), explorando diferentes técnicas, caracterizando-se as partículas formuladas, e analisando-se a sua performance face à adsorção de gases de interesse ambiental.

O MIL-53(Al) foi formulado através de dois metodos diferentes: compressão sem um *binder* (um agente ligante) e extrusão com um *binder*. A partir do método sem *binder* foi obtido duas amostras com forças de compressão differentes,nomeadamente, 1ton-força e 0.5ton-força. O *binder* usado para a extrusão foi o polivinil álcool (PVA),sendo obtidas quarto amostras, com percentagens de *binder* entre 2% e 15% em massa. Os materiais formulados foram caracterizados através várias técnicas mecânicas, estruturais e físico-químicas, assim como também foram medidos os equilíbrios de adsorção de CO_2 de modo a compreender a sua capacidade de adsorção nos materiais. A performance das partículas foram depois comparadas com a capacidade de adsorção de CO_2 no MIL-53(Al) em pó. Dos resultados obtidos, conclui-se que as amostras com as melhores características para aplicar em processos de adsorção gasosa de CO_2 são as formulações sem *binder* com

uma compressão de 0.5ton-força e a amostra com 5% de PVA *binder*. Em geral, ambos os métodos mostram potencial para dar forma ao MIL-53(Al), e poderão vir a ser uma solução para futuros estudos de scale-up.

Palavras-chave: Equilíbrio de Adsorção Gasosa, Materiais Adsorventes, *Metal-organic frameworks* (MOFs), Dióxido de Carbono CO_2, Formulação *shaping and design* de Adsorventes.

Contents

List of Figures

List of Tables

Acronyms

This list of acronyms only specifies the most important ones

CCS Carbon Capture and Storage.

ESA Electric Swing Adsorption.

GHGs Greenhouse Gases.

lp large pore.

MIL Materials Institute Lavoisier.

MOF Metal Organic Framework.

np narrow pore.

PSA Pressure Swing Adsorption.

PVA polyvinyl alcohol.

TGA Thermogravimetric Analysis.

TSA Temperature Swing Adsorption.

XRD X-Ray Diffraction.

Chapter 1

Introduction

1.1 Motivation

Over the last decades global warming and climate change have been environmental issues with a growing concern. Today due to great scientific evidence it has been confirmed that greenhouse gases (GHGs) are the main cause for the rise of the mean global temperature [1, 2, 3]. This temperature will lead to global climate changes with irreversible consequences on the environment and world economy [2, 4]. Therefore, it is necessary to significantly cut and mitigate greenhouse emissions.

In December 2015, the international community composed by more than 185 countries agreed on a new global climate change agreement (Paris Agreement), with main goal of keeping the mean global temperature rise below 2ºC (above pre-industrial levels)[1, 5]. This commitment had already been taken by the European Union (EU) and is a part of the EU's Europe 2020 and 2050 strategies to turn the EU into a "low-carbon" economy [6]. Europe has already decreased their greenhouse emissions by 19% (since 1990 levels), showing that it is possible to change the trends [4, 6]. However, this commitment will only be possible to accomplish with great effort, and various strategies must be applied in order fulfil these goals.

GHGs are composed mainly by carbon dioxide (CO_2), methane (CH_4), nitrous oxide (N_2O) and fluoridated gases. The largest percentage of these emissions belong to CO_2, which account for about 76% of all greenhouse emissions worldwide [3]. The main path into decreasing GHGs emissions and in particular CO_2 is by reducing the use of fossil fuels and lowering industrial emissions, since these contribute to about 65% of all CO_2 emissions [3, 4]. Although, Europe and other countries worldwide have been an example at lowering their emissions, globally GHGs are still increasing. For the past decade CO_2 emissions have had an annual average increase of 2.7% and at this rate it is estimated that

the global temperature will rise well above the 2ºC target [2, 7].

Nowadays humankind has a great and growing demand on energy and we are totally dependent on its supply, as it is the backbone of all modern economies. Today more than 80% of energy supply comes from fossil fuels such as crude oil, coal and natural gas [8]. This is mainly due to the availability and relatively cheap cost of these fuels compared to alternative energies [3, 4, 8]. As stated, a need for alternative energy sources is crucial, but also other strategies are in need in order to ensure a secure energy supply while changing into a low-carbon energy supply system.

Carbon Capture and Storage (CCS) is considered to be a mid to long term strategy for cost effective CO_2 capture for power plants and CO_2 intensive industries [7, 9, 10]. CCS consists in three steps: capture, transport and storage of CO_2, where the most expensive stage is the capture that represents two thirds of the total cost of CSS [9, 11, 12]. The most common technology for CSS is absorption processes such as amine-based scrubbing, which is a well established technology with high CO_2 recovery rates (up to 95%). However, there are drawbacks to this process, such as the production of wastewater, high energy demands and the solvents used are corrosive and degrade during the process [7, 9, 12]. Therefore, different technologies must be developed in order to make CCS processes more efficient.

Adsorption-based separation processes are one of the potential alternatives for CO_2 capture [7, 12, 13, 14]. Gas adsorption is carried out by the use of a solid adsorbent, in which the gaseous fluid phase adsorbate attaches itself either physically or chemically [12]. The separation of CO_2 and other gases using adsorption can be achieved by using different processes, that are usually carried out in a fixed bed system, which has basically two main steps: adsorption and regeneration [15]. Regeneration occurs when the adsorbates are removed or recovered from the adsorbent, thus allowing the solid to be used multiple times [11, 15]. Different adsorption technologies are used to apply adsorption processes and mainly diverge on the regeneration step. As an example the most commonly used and mature process is dominated as Pressure Swing Adsorption (PSA), in which the adsorbent regeneration is carried out through reduction of the total pressure in the system [15]. Other examples of adsorption processes used for CO_2 capture are Temperature Swing Adsorption (TSA) and Electric Swing Adsorption (ESA)[7, 9, 12, 16]

The advantages of adsorption processes is that there are no by-product production such as wastewater and they are potentially less energy demanding compared to absorption processes [9, 17]. Although there are clear advantages with adsorption processes for CSS there are still limitations compared to other well established technologies. Those limitations may lay on different factors such as operating temperature, selectivity, capacity and regeneration of the adsorbent, CO_2 removal efficiency, costs and scale-up of processes [9, 14]. In order to overcome these obstacles one important factor is the selection of a proper adsorbent for CO_2 capture. Therefore, it is of paramount importance to develop and study a wide range of different adsorbents and their applicability in CCS processes [14, 16].

A vast number of different adsorbents show potential in CO_2 capture. Metal Organic Frameworks (MOFs) are a relatively novel class of materials that are now subject to different studies and in particular in gas adsorption processes [11, 14, 16, 18, 19, 20, 21]. Only recently some MOFs been available commercially but are still generally only commercialized in their powder form. If a powdered adsorbent, for instance a MOF, were to be used in a adsorption process, such as PSA, different problems would arise, such as high pressure drops [18, 22, 23, 24, 25]. Therefore, it is necessary to shape an adsorbent into body like forms, such as pellets or extrudates to overcome these problems and further study their applicability in these processes. Here arises the main goal of this thesis, which is to shape adsorbents, and in particular MOFs, with different techniques and study their characteristics and applicability for adsorption processes.

The objective of this dissertation is to understand what different kinds of shaping techniques and which optimized conditions can be applied to shape adsorbents, which in this work was the MIL-53(Al) MOF. Different mechanical, structural and physico-chemical analysis are performed in order to characterize the obtained particles. Furthermore, these shaped materials are also characterized through CO_2 adsorption equilibrium measurements as it is essential to understand the viability of applying these materials in alternative CSS technologies.

1.2 Structure of the Dissertation

This dissertation is divided into five chapters.

- **Chapter 1:** Introduction.

  This chapter demonstrates the motivation of the dissertation. The intent is to show the problems and issues related to the excess of carbon dioxide emissions and how adsorption processes and adsorbent materials are possibly viable alternative solutions. This chapter also summarizes the organization of this work.

- **Chapter 2:** Theoretical Background. This chapter comprises the review of the theoretical background regarding adsorption phenomena, adsorbents and in particular MOFs, such as MIL-53(Al). This chapter also includes a review of different shaping techniques for porous materials and the different characterizations that should be performed in order to fully characterize a shaped adsorbent.

- **Chapter 3:** Methodologies and Experimental Work. This chapter shows the different methods and experimental work carried out. It starts by showing the two different shaping techniques used, followed by the description of the different methods employed to characterize the different shaped materials.

- **Chapter 4:** Experimental Results and Discussion. This chapter presents the results and analysis of the experimental work performed. The two different methods were

used to shape the MOF MIL-53(Al) are discussed and compared. The different characterization analysis of the samples and adsorption equilibrium measurements are also reported.

- **Chapter 5:** Conclusions and Future Work. This chapter summarizes the work done in this dissertation and presents a conclusion from all the work developed and from the results obtained. Furthermore, it discusses potential future work that may enhance the work done in this dissertation.

Chapter 2

Theoretical Background

2.1 Adsorption Phenomena

Nowadays adsorption phenomena is a part of numerous important processes in different technological applications [26]. The use of adsorption techniques are a part of our civilization dating all the way back to ancient Egypt and Japan, where wood char was already used to purify medicinal substances, yet only in 1881 was the term adsorption first introduced by Kayser [26, 27].

Today most of the attention regarding this phenomena focuses on its practical application in industries and in environmental protection [15]. Adsorption has a wide range of industrial applications, such as separation and purification of liquid and gas mixtures, bulk chemicals and isomers; drying gases and liquids; removal of impurities; recovery of chemicals from industrial vent gases and also gas storage [11, 15, 28].

The adsorption phenomena can be defined as adhesion of gas or liquid molecules on the surface of a solid adsorbent [27, 29]. In a mixture, each component of a gas or liquid (adsorbate) has a different affinity towards the surface of an adsorbent, thus separation is achieved duo to a higher affinity of the adsorbate to the adsorbent. [29, 30]. Different types of phenomena can occur during adsorption, mainly due to different bondings between the adsorbate and the adsorbent [31]. Depending on these different interactions and energy between the bonds of the molecules can be divided into two different categories: physical adsorption (physisorption) or chemical adsorption (chemisorption) [11, 31].

Physisorption relies on Van der Waals and electrostatic forces that occur between the adsorbate and the adsorbent [11, 31]. These bonds are relatively week and also since no chemical reaction occurs and no chemical bonds are created, this type of adsorption is more easily reversible (desorption) and the adsorbed molecules preserved and keep their

original identity [31, 32].

Chemisorption occurs due to chemical reactions that creates stong bonds between the adsorbate and the adsorbent [31]. As a result, since there are chemical bonds, the adsorbent loses its original identity. Therefore, desorption may not possible in this type of process [31, 32].

Adsorption depends on two parameters temperature and pressure (or concentration). Physisorption of gases are commonly reported through adsorption isotherms [33]. An adsorption equilibrium isotherm at constant temperature is the relationship between the amount adsorbed by unit mass of solid and the equilibrium pressure of the gas. This is, the equilibrium between the amount adsorbed q and the partial pressure p of the adsorbate at a constant temperature T (Equation 2.1)[27, 33]. This equilibrium shows to which extent the solute is adsorbed in the selected conditions [30].

$$q = q(p) \qquad \text{(at constant } T\text{)} \tag{2.1}$$

Different type of physisorption isotherms can occur in gas adsorption, for various adsorbent-adsorbate pairs. Five experimental isotherms for pure gases were identified by Brunauer in 1940. The IUPAC recommends a classification based on 6 types of isotherms as shown in Figure 1 [33] . The first five types, I to V, were proposed in 1940 by Brunauer, Deming, Deming, and Teller and they are referred to as BDDT classification [15, 34]. There are a considerable number of borderline cases that are difficult to assign to one group rather than another. The recommended IUPAC classification is expressed as being types: I(a), I(b), II, III, IV(a), IV(b), V and VI [33].

- **Type I,** this type of adsorption isotherm corresponds to a mono-molecular adsorption, forming a mono-molecular layer of adsorbate. It presents a maximum limit of the amount adsorbed. Furthermore, this isotherm is typical of gases that are above their critical temperature [27, 30]. Type I(a) isotherms are typical of microporous materials having mainly narrow micropores (approximately < 1 nm); Type I(b) isotherms are found with materials having pore size distributions over a broader range (approximately < 2.5 nm) [33].

- **Type II,** this type of adsorption corresponds to a multi-layer BET adsorption. This type of adsorption occurs by layers, in which the heat of adsorption for the first adsorbed layer is higher than for the subsequent layers. Moreover, each layer is assumed to have a heat of adsorption equal to the heat of condensation. Usually this type of isotherm presents with gases at temperatures below their critical temperature and for pressures that are bellow and approaching their saturation pressure [27, 30].

- **Type III,** this type of adsorption also corresponds to a multi-layer BET adsorption. This adsorption also occurs by layers, but in this case the heat of adsorption of the first layer is lower than the subsequent layers. This isotherm shows that as the

heat of adsorption of the first layer approaches zero, adsorption is delayed until the saturation pressure is approached. Furthermore, this isotherm is quite undesirable, due to its low adsorption capacities at low pressures [30].

- **Type IV and V,** these types of adsorptions correspond to the capillary condensation versions of type II and III isotherms, respectively. Adsorption in these isotherms occur before before saturation pressure is reached. In the case of type IV(a) this isotherms demonstrate the phenomena of hysteresis. Hysteresis occurs in multi-molecular adsorption regions, in the figure it is shown by the upward adsorption branch due to simultaneous multi-molecular adsorption and capillary condensation. The downward branch is the desorption. This can also occur in other isotherms if impurities are present [30, 33].

- **Type VI,** corresponds to a reversible stepwise isotherm, this is a layer-by-layer type of adsorption on a uniform nonporous solid. Each step represents a layer of adsorption capacity[33].

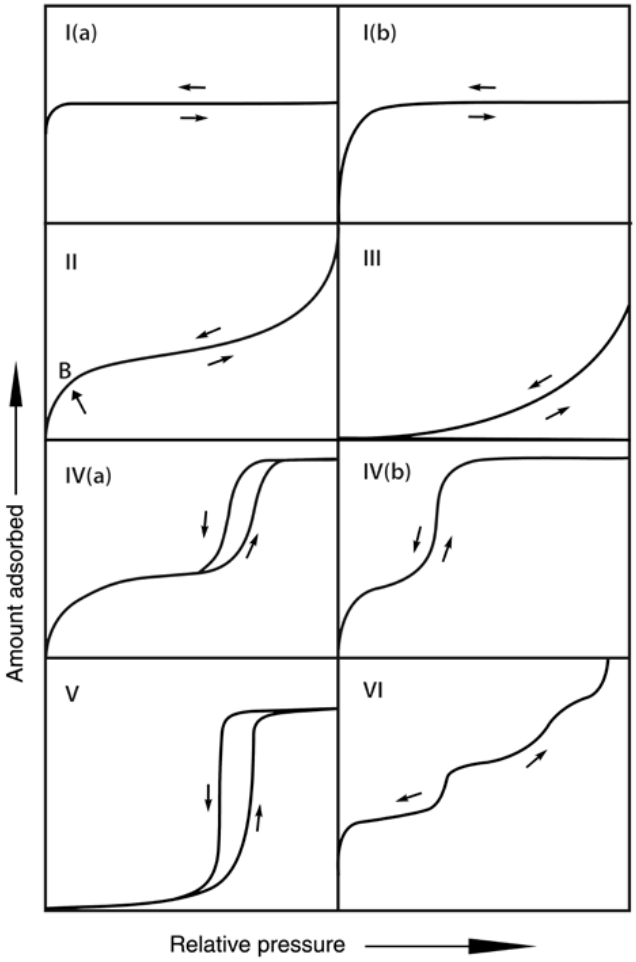

Figure 2.1: IUPAC classification of physisorption isotherms [33].

To further study adsorption, different techniques may be applied depending on the characteristics of the adsorbate, adsorbent and the desired conditions.

2.2 Adsorbents

Many different materials have been developed for gas separation, the most commonly known are: activated carbons, silica gel, ion-exchange resins, zeolites, mesoporous silicate, activated alumina and metal oxides [11, 26, 34]. Moreover up until the XX century only 4 types of adsorbents were commercially sold: activated carbon, zeolites, silica gel and activated alumina [34].

Recently new adsorbents have emerged showing more promising results in gas adsorption, such as carbon fibers, carbon nanotubes, graphite nanofibers, mesoporous molecular sieves and Metal Organic Frameworks (MOFs) that have high surface areas and are very porous materials [11, 34]. However, these materials, are quite expensive essentially due to their raw material cost and are only commercially available as-produced powders and not in the proper form for process gas separation [35]. Further research is needed to develop these new adsorbent materials to their full potential [34].

Selecting an appropriate adsorbent is one of the most fundamental and critical steps in gas adsorption processes [36]. However, this selection is a quite complex problem, because it involves looking for different attributes [34]. Important attributes that should be analysed when selecting an adsorbent are:

- **Selectivity,** this attribute can be based on three factors: affinity, kinetic selectivity and pore size. Affinity is the adsorbents affinity to the target molecules that are desired to be adsorbed. Kinetic selectivity is the intraparticle diffusion rate, this defines the rate at which different components diffuse into a pellet. Size and shape of the pores of an adsorbent are also a critical factor when choosing an appropriate adsorbent. The selected material should shave a small pore size, but large enough to accommodate the desired adsorbate [27, 34]. These three factores combined or independently define the selectivity of an adsorbent for a desired adsorption [27].

- **Capacity,** of an adsorbent depends on the nature of the material, the nature of the pores and the working conditions [28]. Adsorption is widely dependent on the interfacial area. Therefore, when selecting an adsorbent it should show a high capacity of adsorption, this depends mostly on its surface area, that usually should be well over 100 m^2/g [26, 27]. These type of materials are usually very fine particles or highly porous to achieve better results, between a micropore range and a macropore range [26, 36]. The classification of pore sizes recommended by the International Union of Pure and Applied Chemistry (IUPAC) is shown in Table 2.1.

- **Regeneration,** also known as reversibility of adsorption is a condition that can be desired if the adsorbent is to be reused or if the adsorbed substance is also to be

recovered [27]. This factor is significant when determining if the chosen adsorbent is efficient for the desired process or not, because it is directly associated to the cost of the process [28]. In some cases the same adsorbent may be reused for months or even for years [27]. Regeneration can be evaluated, for example, by temperature or pressure swing and by the energy required [34].

Table 2.1: Classification of pore sizes by IUPAC [36].

Micropores	$d < 2nm$
Mesopores	$2nm < d < 50nm$
Macropores	$d > 50nm$

2.2.1 Metal Organic Frameworks

Coordination polymers are in general materials in which a material possesses an extended connection of metal and ligand monomers through coordination bonds [19]. In this category we can find Metal Organic Frameworks (MOFs) that have the particularity of showing strong bonding, linking units and a geometrical highly ordered structure [19, 37]. MOFs are a new class of materials that were developed just about three decades ago [28, 38, 39]. For the last two decades (MOFs) have been more intensely developed and have been showing great potential for several applications such as in gas storage, gas adsorption, magnetic materials, luminescent and florescent materials, sensors and in drug storage and delivery [18, 19, 28, 38, 39, 40, 41].

MOFs can be described as being a "hybrid porous solid, in which the framework is ensured by the linkage of inorganic moieties with functionalized organic molecules through covalent or iono-covalent bonds" or as "organic-inorganic hybrid solids with infinite, uniform framework structures build from organic linkers and inorganic metal nodes" [28, 42]. Figure 2.2 shows a summarizing representation of the general classification of porous solids [28].

Today one of the best examples of the importance of porous material in industrial processes are zeolites, which already have a major role in chemical processes and other industrial applications [19, 28, 35, 38, 39]. MOFs are many times compared to zeolites due to their similarities in nature and structure. However, MOFs are captivating more interest, due to their greater versatility compared to other adsorbent materials [18]. This versatility is due to their framework structures and pore properties that can be tailored by choosing appropriate metal and ligand constituents [39, 43].

One of the most interesting properties that MOFs possess are their porosity. With higher porosity and larger surface areas, in comparison with other traditional porous materials (e.g. activated carbons and zeolites), they are great options for the accommodation of different foreign chemical entities (e.g. H_2, CO_2, CH_4). Hence their applicability in processes of gas storage and gas separation [16, 19, 21, 28, 38, 42].

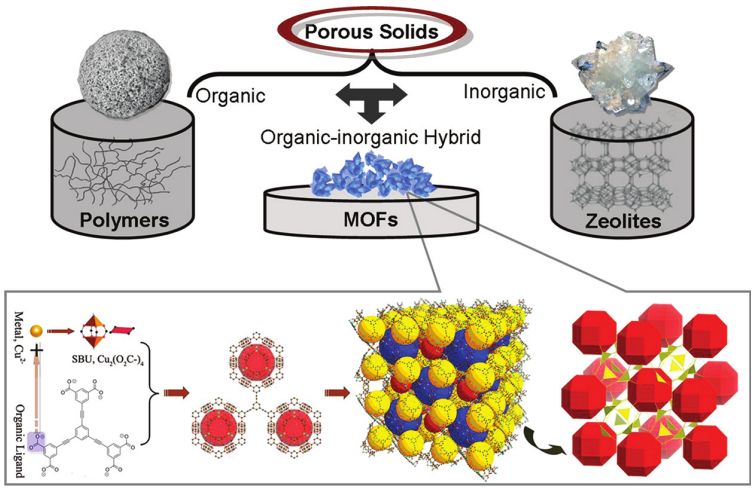

Figure 2.2: Representation of the general classification of porous solids [28].

2.2.1.1 MIL-53 (Al)

MIL-53(Al), also known as aluminum terephthalate, is a MOF that attracted attention for gas adsorption, especially due to its great flexibility and capacity to adsorbs large amounts of gases, such as H_2, CO_2 and light alkanes [39, 44, 45]. This material is part of a class of MOFs that are classified as porous metal carboxylates of the MIL-n type, where MIL stands for Materials Institute Lavoisier. The MIL-53 framework is highlighted due to its great flexibility and ability to assume different pore conformations that is induced when hosting different molecules, by temperature changes or by mechanical pressure [40, 45, 46, 47].

The flexible nature of this framework or "breathing capacity" is mainly due to transitions that oscillate between two forms: a large pore (lp) and a narrow pore (np) (Figure 2.3). Furthermore, the transition between each form can have a difference in cell volume up to 40% [17, 39, 44, 45, 48]. This breathing transition and behavior can be induced by different factors, such as the adsorption of different types of molecules, temperature changes and mechanical compression [44, 47, 49]. For example, at 30ºC the MIL-53 framework will transition between np and lp during adsorption of CO_2 and H_2O, but during adsoprtion of H_2 and CH_4 this does not occure [16, 50]. Furthermore on commercialized MIL-53(Al) this breathing behaviour has not been reported [16, 51].

In gas adsorption processes MIL-53(Al) has been object of study for the last few years. Promising results have been shown with this MOF in adsorption of different gases such as CO_2, CH_4, CO_2/CH_4 mixtures, N_2, of supercritical methane and of Xenon (Xe) [16, 25, 39, 44, 45, 48, 51, 52, 53, 54].

The first company to commercialize MOFs was Basf, back in 2008 [55]. MIL-53(Al) is now produced by Basf under the trade name Basolite® A100 [17].

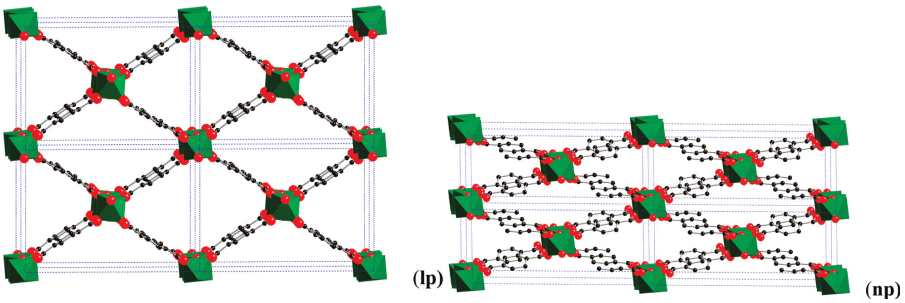

(a) Metastable large pore (b) Metastable narrow pore

Figure 2.3: Representation of the metastable large pore (lp) and narrow pore (np) structures of the MIL-53(Al) material, as a 2 × 2 × 2 supercell viewed along the axis of the unidimensional channel [45].

2.3 Shaping Techniques for Gas Adsorption Applications

Most porous materials such as MOFs are synthesized as a powder, but in order to apply them in processes such as fixed-bed gas adsorption these powders must be transformed or shaped into bodies known as extrudates, beads or pellets [18, 22]. Moreover shaping MOFs and other novel porous materials bring these materials a step closer to the use in industrial processes [24, 56].

By giving shape to these materials it is possible to obtain structures that can be used in processes that help achieve lower pressure drops, better heat management and higher mechanical stability [23, 24, 25]. The major challenge in shaping adsorbents is to maintain at its best, the original properties and characteristics of the powder material and a desirable mechanical resistance, in order to their proper usage in typical gas adsorption processes applications. [18, 57]. Many different properties relate to the performance of these structured materials, but tradeoffs between these parameters are inevitable [23]. For example, with smaller pellets you can achieve faster mass transfer but this will lead to higher pressure drops in packed beds [23].

Techniques to produce structured materials from powder materials are more or less similar to ceramic processing. Some of these are known as extrusion, coating, colloidal processing, templating and dry pressing, [23, 41]. Extrusion of pellets and honeycombs is one of the most widely used process to shape porous powders, this type method is represented in Figure 2.4 [23, 58, 59]. Furthermore, it is an established industrial process in producing pellets and monoliths of already widely commercialized adsorbents and catalyst (e.g.: zeolite A, X, ZSM-5)[23, 58]. Pelletization is the process in which a material is enlarged into a millimetric agglomerate (pellets) with low intra-agglomerate porosity (about 10%) [18, 60]. Usually these pellets have a size ranging between 0.5 to 2mm [60].

Coating, colloidal processing, templating and dry pressing are other well known process to shape porous powders. Coating is a process in which a supporting shaped material (e.g.: coated honeycomb) is coated with the adsorbent particles [23]. This type of shaping

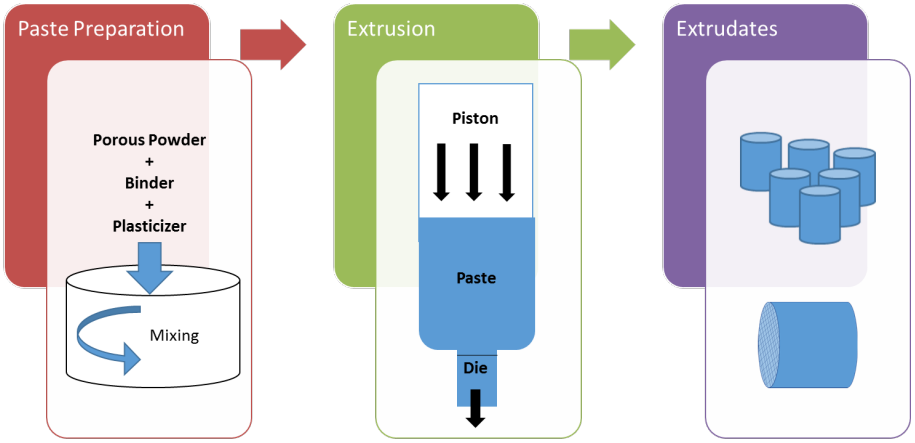

Figure 2.4: Representation of an extrusion method.

overcomes heat transfer and pressure drop limitations compared to traditional extruded pellets. Colloidal processing is used to obtain macroscopic monoliths or bodies by dispersing the powders into a liquid or a polymer. Templating techniques can be generally defined as a process in which a structured mould is used to shape a materiel [61]. These techniques are varied and can be differentiated as soft templating, hard templating and solvent templating [23]. Dry pressing is another widely used technique, where a powder is compacted through a metal die to form a desired shape, as represented in Figure 2.5 [57, 62].

These techniques can be divided into two distinct categories: without binder (binderless) or with binder. Being that a binder is material that binds other materials together, acting like a glue or as an adhesive between particles [18].

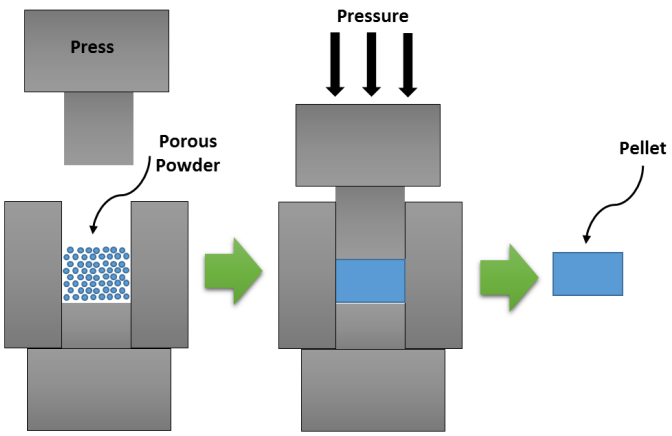

Figure 2.5: Representation of a dry pressing method.

2.3.1 Binderless Shaping

Binderless shaping relates to the process of transforming porous materials into shaped macroscopic bodies without the aid of binders [23]. The most common technique to shape porous powders, without a binder is by compression, in which the material is compressed together and creates a physical bond. The simplest way to achieve this is by pressing the material into pellets by use of a press and then these pellets can be crushed and sieved into a desired size, see image [22, 25, 63]. Previously other MOFs have been shaped using this method with different pressures: MIL-53(Al) with a pressure of 500bar and $Cu_3(BTC)_2$ with 25.33 bar [25, 63]. Although this method has the advantage of not using a binder that will inherently change the properties of an adsorbent, with the use of high pressures to shape structured adsorbents a possible degradation of their crystal structure is an issue [18, 57, 63]. Therefore further studies to understand the impact of this type of shaping on MOFs is necessary.

A more novel technique that has been applied to different porous materials is by the use of Pulsed Current Processing (PCP), which uses high heating rates to partially fuse porous particles together [23]. The PCP process provides has been successful for many porous materials but since its heating process is very high (approximately 800ºC) this may not be applicable to some materials that are not resistant at high temperatures [18, 23].

2.3.2 Shaping with Binder

Shaping a porous material with aid of a binder is usually is achieved by blending the powder with an inorganic or organic binder and a liquid phase (plasticizer) into a paste [59, 64]. In general, to achieve high mechanical strength, inorganic binder is used, while an organic binder is used when a certain plasticity and mechanical strength is desired [59, 64]. The advantage of using a binder, for example in extrusion, is that the porous powders easily form into desired shaped and usually without the use of pressure [65]. The drawback using a binder is the fact that it also reduces the mass percentage of the adsorbent powder in a shaped body [65].

A wide range of binders have been used to structure porous powders. The greatest problem is to chose an appropriate binder and plasticizer for the material in hand. Furthermore, obtaining an adequate proportion between binder and powder is another challenge itself. In the case of shaping MOFs, the goal is to mix just enough binder to obtain good mechanical stability while maintaining a high specific surface area [59].

The most common inorganic binders used for porous solids are alumina and silica oxides, kaolin and siloxanes. Organic binders that are also commonly applied are cellulose, methyl cellulose and polyvinyl alcohol (PVA) [23, 59]. When choosing an appropriate plasticizer usually the first choice is water, which is easily removed by evaporation. However, if the powder used dissolves in water (e.g.: UTSA-16) organic solvents or organic-water mixtures can be used [59].

PVA shows particular interest as a binder for adsorbents, including MOF materials. PVA is a thermoplastic and biodegradable synthetic polymer that is soluble in water. PVA shows good properties as a binder, with low toxicity, anti-electrostatic properties, chemical resistance, toughness and permeability [59, 66]

This binder has been previously applied to shape adsorbents and shows promising results with different MOFs, such as: MIL-53(Al), UTSA-16 and $Cu_3(BTC)_2$ [25, 59, 63].

As discussed, the amount of binder applied to an adsorbent is a critical issue, because an excess of binder will decrease considerably the surface area, while too little will not give the mechanical and physical strength desired. It is suggested that the ideal amount of PVA should be used from 1 to 5% (2% is preferred) by weight of PVA based on the total weight of the adsorbent (w/w) [66]. This should give the adsorbent the desired hardness and adsorption capacity. In a previous study with MIL-53(Al) the surface area did decrease to a great extent when using over 10% (w/w) of PVA as a binder [25]. Most recently a research was developed with UTSA-16 showing better results with this binder as different and lower percentages of binder were studied [59].

In conclusion, further studies of different mixtures and shaping techniques with binders should be conducted for different MOFs in order to achieve desirable shaped bodies that maintain to its best the materials original properties.

2.4 Characterization of Shaped Adsorbents

When shaping materials, an important step is to evaluate the different characteristics of the shaped material. In the case of adsorbent powders for gas adsorption, equilibrium experiments are conducted to determine the materials adsorption capacity and specific surface area. Other important properties that must be tested are mechanical, structural and physico-chemical characteristics. The determination of these different parameters can give an overall image of the material and validate its usage in gas adsorption processes.

2.4.1 Mechanical Characterization

Shaped materials used in gas adsorption processes will be subjected to different conditions that may lead to deterioration of its structure and thus leading to poor results. Adsorbents used in gas adsorption processes are generally used in fixed bed systems. In order to fill a column with shaped adsorbent it must be packed in order to achieve maximum surface area, during the process the particles will be subject to very high pressure changes and different temperature ranges which can degrade the material. Therefore, a mechanical analysis must be conducted in order to assess if the material will withstand and maintain its form during gas adsorption processes. Tests that can be used to characterize a structured adsorbent are: pressure/depressurization, compression, drop and abrasion tests.

2.4.2 Structural and Physico-chemical Characterization

In the case of porous adsorbent materials such as MOFs it is essential to analyse their structure in terms of porosity and physical chemical properties. When shaping porous materials either with or without the use of a binder the stucture of the material can change as well as its physical and chemical properties. In order to analyse these properties different methods can be used such as: Scanning Electron Microscopy (SEM) imaging, X-Ray analysis (XRD) and mercury (Hg) porosimetry, thermogravimetric analysis (TGA) and nitrogen (N_2) adsorption.

2.4.3 Adsorption Equilibrium Measurement Techniques

Adsorption equilibrium measurements are used to determine the adsorption capacity of an adsorbent under certain conditions. They are effective to understand the materials adsorption properties in different pressure and temperature conditions. Various techniques have been developed for adsorption equilibrium measurements of gases. Two well known methods are the volumetric/manometric and gravimetric, each presenting advantages and disadvantages.

- **Volumetric,** also known as gas adsorption manometry or as the BET volumetric method, is based on the measurement of the gas pressure in a calibrated, constant volume (at constant temperature) [26]. It is the oldest and most simple method to determine adsorption isotherms [31]. The apparatus for this method can have different configurations, but in general the layouts are simple and follow the same principle. During a volumetric experiment a known amount of adsorbate gas is expanded into a confined, calibrated volume containing the adsorbent, which is maintained at a constant temperature. Once the adsorbate and the adsorbent are in contact adsorption starts to occur and the pressure in the volume falls until equilibrium is achieved. The difference between the initial and the final volume of gas gives us the amount of volume of the adsorbate that was adsorbed [31]. Advantages of this system is its simplicity and relatively low cost to build [67]. Although due to its more simplistic approach it shows some disadvantages. This method does not perform very well in lower pressures and the precision of the data is lower than compared to other methods, such as the gravimetric method [31, 33].

- **Gravimetric,** is a method also used to study adsorption phenomena, which consists in weighing the porous adsorbent material in a highly sensitive balance. This balance, which can be a microbalance, is able to measure small relative changes in the weight of the adsorbent during the adsorption process. Gravimetric adsorption measurements are used to characterize porous media, to measure gas adsorption equilibria and to investigate adsorption kinetics. The greater advantages to this method are its accuracy, and its performance with extreme pressures. The microbalances used today are give highly accurate and sensitive compared to other systems.

The main disadvantage to this method is that the equipment is more complex and consequently more expensive. Furthermore a microbalance is sensitive to electromagnetic and mechanical disturbances that may oscillate the balance and cause experimental problems during adsorption equilibria measurements.

Chapter 3

Methodologies and Experimental Work

This chapter is divided into two main parts. The first part consists in the description of the two methods employed to shape MIL-53(Al). The second part describes the characterization techniques used.

3.1 MIL-53(Al) Shaping

The main objective of this thesis is to shape an adsorbent for application in adsorption processes. The MOF MIL-53(Al) will be the adsorbent under study in this work. This adorbent was purchased from Sigma-Aldrich (product no.688738) with the trade name Basolite® A100 (synthesized by BASF AG, Ludwigshafen, Germany). Basolite® A100 is sold in a powder form, its surface area is reported to be between 1100-1500m^2/g, with a bulk density of 0.4 g/cm^3 and with a particle size distribution of 31.55μm [68]. Furthermore, since its production some researchers have studied and applied Basolite® A100 in adsorption processes and have confirmed the material characteristics reported by the manufacturer [16, 44, 51, 53].

Two different methods were used to shape this porous material: binderless compression and extrusion with binder. Initially both methods were first tested with activated charcoal in order to get a better understanding of how each process should be carried out on a cheaper adsorbent material. Activated charcoal generally costs less than 0.20€/g , while Basolite® A100 costs 8.85€/g. Only visual results were taken into account and no further studies with activated charcoal were done, as it is out of the focus of this dissertation.

3.1.1 Binderless Shaping

To create samples of binderless pellets a manual hydraulic press (15Ton manual hydraulic press, Graseby Specac) with a circular evacuable pellet die with 10mm diameter was used (Figure 3.1). Each sample was weighed (approximately 0.5g) and inserted into the pellet die.

Preliminary tests were done with activated charcoal in order to understand what pressures should be used on the MOF. The press used has a scale in ton-force (tf) and has a minimum force of 0,5tf and a maximum 10tf, which is approximately 624bar and 12482bar respectively. To convert the force applied into pressure the equation 3.1 was used, where: P_{bar} is the pressure in bar, F_{tf} is the force in ton-force, d is the diameter of the pellet in meters and 10.2 corresponds to the conversion of 1 bar to ton/m^2[69].

$$P_{bar} \simeq \frac{\frac{F_{tf}}{(d/2)^2\pi}}{10.2} \tag{3.1}$$

Figure 3.1: Manual hydraulic press and pellet die.

Different samples were made applying different forces from 0.5tf to 10tf for 10 minutes. The results obtained with activated charcoal can be seen in Table 3.1 and in Figure 3.2. From observation it was concluded that with forces above 1tf the activated charcoal pellets were less consistent and more brittle than the 0.5tf and 1tf pellets.

Two different forces were selected for the binderless MIL-53(Al) samples: 0.5tf (≃624bar) and 1tf (≃1248bar). Each of these samples were left in the press for 10 minutes, while the desired force was applied. After removing the formed disks from the press they were crushed and sieved the desired size. All the samples were crushed with the aid of a hammer and sieved with sieving trays between 1mm and 2mm sieves. This process was repeated several times until the desired amount of granulates of MIL-53 were obtained. Table 4.1 summarizes the binderless samples produced with this method.

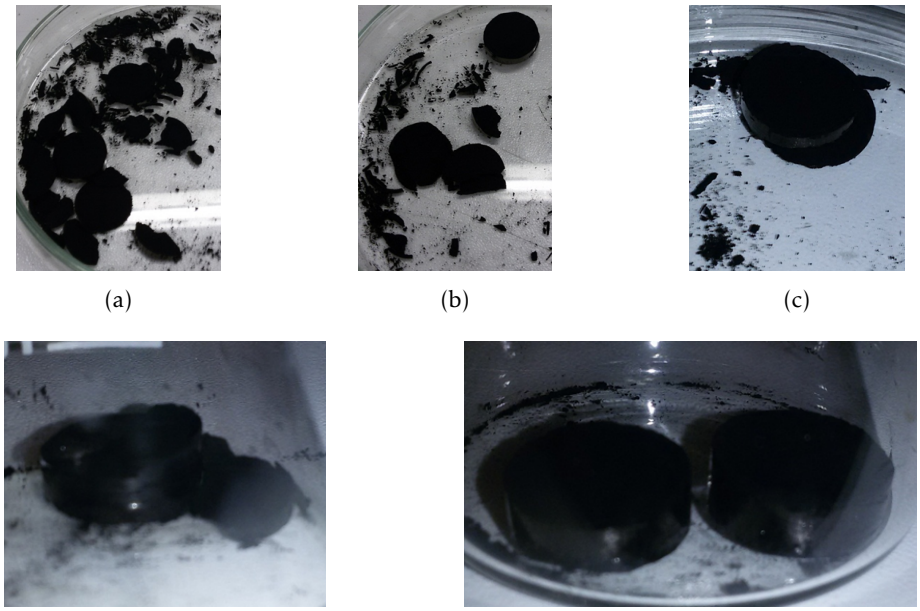

(a) (b) (c)

(d) (e)

Figure 3.2: Activated Carbon Binderless Disks: (a) Batch Y1 & Y2; (b) Batch Y3 & Y4; (c) Batch Y5; (d) Batch Y6; (d) Batch Y7 & Y8.

Table 3.1: Binderless Activated Charcoal Pellets Samples and Results.

Batch	Force (tf)	Pressure (bar)	Observations
Y1 & Y2	10.0	12482	Pellets are very brittle
Y3 & Y4	5.0	6241	Pellets are very brittle
Y5	1.5	1872	Pellet with more consistency but a little brittle
Y6	1.0	1248	Pellet with more consistency but a little brittle
Y7 & Y8	0.5	624	Pellets with more consistency

Table 3.2: Binderless MIL-53(Al) Samples.

Batch	Force (tf)	Pressure (bar)	Sieve (mm)
A1	1	1248	1-2
A2	0.5	624	1-2

3.1.2 Shaping with Binder

In order to shape MIL-53(Al) with a binder, the first step is to select the appropriate binding agent. As discussed previously in Chapter 2, PVA has favourable properties to act as a binder for MOFs [59, 66]. Therefore PVA was the selected binder used in this method. Afterwards, a method for mixing and extruding the MIL-53(Al)-PVA mixture was developed. As in the binderless method, preliminary extrusion tests were carried out with activated charcoal.

3.1.2.1 PVA Solution Preparation

A PVA solutions are basically obtained by mixing PVA and distilled water. This polymer was purchased from Sigma-Aldrich (product no.10852) with the trade name Mowiol® 10-98(synthesized by Sigma-Aldrich, Steinheim, Germany).

PVA is initially mixed with cold distilled water in small amounts at ambient temperature and under stirring. In order to solubilize completely the PVA, this solution must be heated up to a temperature range of 90ºC to 98ºC with continuous stirring [70]. Ideally, in order to insure that no water is lost by evaporation, this process should be carried out with in a three necked flask adjusted with a reflux condenser, a thermometer and a mechanical stirrer [25, 63]. Alternatively, as a three necked flask was not available, only a beaker, a magnetic stirrer and a thermometer were used. Heating was obtained with a magnetic hotplate stirrer (VMR-VMS-C7). During the heating process, the beaker was covered with tin foil in order to avoid water loss and the temperature was measured by the use of a thermometer. The mixing time varied from 2 hours to overnight depending on the amount of PVA being solubilized.

Four solutions were prepared with different weight/weight percentages from 2%(w/w) to 15% (w/w). The PVA solutions prepared and the amount of water and PVA employed are shown in Table 3.3.

Table 3.3: PVA Solutions Prepared.

Batch	**PVA Solution (% w/w)**	**PVA (g)**	**Distilled Water (g)**
PVA2	2	0.51	25
PVA5	5	1.32	25
PVA10	10	2.78	25
PVA15	15	4.41	25

3.1.2.2 MIL-53(Al)-PVA Mixture and Extrusion

The amount of binder applied to MIL-53(Al) is a critical issue, if too much is employed the surface area of the adsorbent will decrease considerably, while if too little is used the material will not possess the mechanical resistance desired. The ideal amount of PVA to be used as a binder ranges between 1% and 5% [66]. Alternatively, previous studies with MOF shaping, suggest that more than 10% of binder can be employed [25, 63]. Therefore, different MIL-53(Al)-PVA mixtures were prepared. This may allow a better understanding of the different characteristics that this adsorbent may have depending on the amount of binder used. Furthermore, this process may permit us to select an ideal amount of PVA that should be used to shape this adsorbent for adsorption purposes.

As a first test, just to understand how extrusion with a syringe would work, two different mixtures were tested with activated charcoal. The details are shown in Table

3.4, here we concluded that the composition of the mixtures will be determinant to origin viscosities that can permit extrusion of the formed paste (Figure 3.3). With sample Z2 we achieved a relatively uniform extrudate using this method (Figure 3.3(b)).

In order to calculate the amount of adsorbent needed to obtain the desired percentage for the mixture equation 3.2 was used, where $W_{adsorbent}$ is the mass of adsorbent used in grams, W_{PVAsol} is the mass of the PVA solution used in grams, PVA_{sol} is the percentage (% w/w) of PVA contained in the PVA solution used and $Binder$ is the total percentage (% w/w) of binder contained in the binder/adsorbent mixture . Any additional amount of water that might be added to the mixture is discarded as it does not affect the percentage of binder in the mixture.

$$W_{adsorbent}(g) = \frac{[W_{PVAsol}(g) \times PVA_{sol}(\%w/w)] \times [1 - Binder(\%w/w)]}{Binder(\%w/w)} \tag{3.2}$$

Table 3.4: Activated Charcoal-PVA Mixtures and Observations.

Batch	Binder (% w/w)	PVA Solution (Batch)	PVA Solution (g)	Activated Charcoal (g)	Observations
Z1	23	PVA15	10.00	5.02	Very fluid mixture and after extrusion did not maintain it's form.
Z2	18	PVA15	15.00	10.25	More viscous mixture and after extrusion maintained it's form.

(a) (b)

Figure 3.3: Activated Charcoal with PVA Binder: (a) Batch Z1; (b) Batch Z2.

Mixtures of the PVA solutions with the powdered MIL-53(Al) were done by simply manually mixing small amounts of MIL-53(Al) in a beaker using a spatula (Figure 3.4(a)). The different mixtures prepared are summarized in Table 3.5, where it is shown that for each batch different mixtures of PVA were used due to their different viscosities. In some situations it was observed that the PVA mixture alone was not sufficiently fluid to disperse the powder, so a small quantity of distilled water was added to the mixture.

(a) (b)

Figure 3.4: (a) Example of a MIL-53(Al)-PVA Mixture; (b) 5ml Syringe used for Extrusion.

Table 3.5: MIL-53(Al)-PVA Mixtures and Samples.

Batch	Binder (% w/w)	PVA Solution (Batch)	PVA Solution (g)	MIL-53(Al) (g)	Added Distilled Water (ml)
B1	2	PVA2	1.250	1.225	2.0
B2	5	PVA2	2.500	0.950	0.0
B3	5	PVA5	1.000	0.950	1.0
B4	10	PVA5	1.500	0.675	0.0
B5	10	PVA10	1.000	0.900	0.5
B6	15	PVA10	1.000	0.566	0.0
B7	15	PVA15	1.200	1.020	1.0

After the preparation of each mixture the following step is to extrude the paste obtained. Extrusion was carried out using a syringe that has an opening of 2mm (Figure 3.4(b)). Each sample was left to dry on a petri dish exposed to air overnight. To ensure that all of humidity was removed from each sample they were afterwards dried in a muffle furnace (Nabertherm B170 GmnH, Germany). The drying temperature was set up to 190ºC with a heating rate of 0.5ºC per minute, near the recommended degassing temperature for MIL-53(Al) and bellow the melting point the PVA which are both at 200ºC [44, 71]. After each sample was completely dried, they were cut into smaller sizes with 1mm to 4mm of length.

3.2 Characterization of Shaped MIL-53(Al)

3.2.1 Mechanical Characterization of Samples

3.2.1.1 Pressure/Depressurization Tests

This pressure/depressurization test were proposed in order to simulate pressure changes that the adsorbent will undergo when packed into an adsorption column. An in-house adaption of a volumetric unit was used (Figure 3.5(a)). The objective of this was to see if the material will withstand mechanically during different cycles with different pressures,

thus simulating similar conditions occurring in adsorption processes such as in a PSA or other fixed bed systems.

The different samples of binderless MIL-53(Al) and MIL-53(Al)-PVA were packed in a small column (Figure 3.5). In the case of the binderless samples they were previously weighed, while for the samples with binder the number of extrudates inserted into the column were counted. The column is then placed in line as represented in the schematic diagram of the pressure test unit as shown in Figure 3.6.

Three different cycles were tested with each sample, at three different pressures of 3, 10 and 18 bar. For each cycle, the pressure in the column is controlled by opening valve 1 (V1) and valve 2 (V2) and checked with the pressure sensor (PT). This pressure transducer is connected to a computer that has a LabVIEW™ (National Instruments software) based software developed in-house which allows to record the instant pressure over time [67]. After the column at the desired pressure, the system is left up to 5 minutes and then depressurized to atmospheric pressure, by opening valve 3 (V3), for another 5 minutes. The process was repeated two more times for a total of 3 cycles. After each cycle the sample was removed from the column, in the case of the binderless samples they were once again sieved between 1mm and 2mm and weighed in order to determine the percentage of material that was fragmented during the each pressure cycle. For the samples with binder they were once again counted in order to determine if any extrudates were damaged or broken.

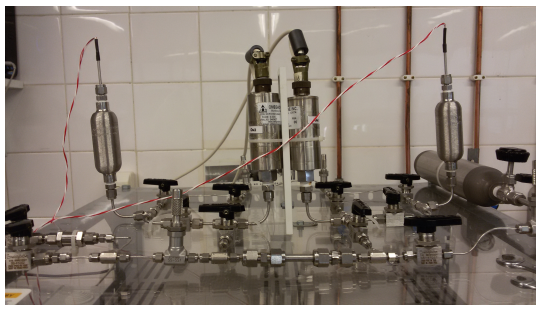

(a)

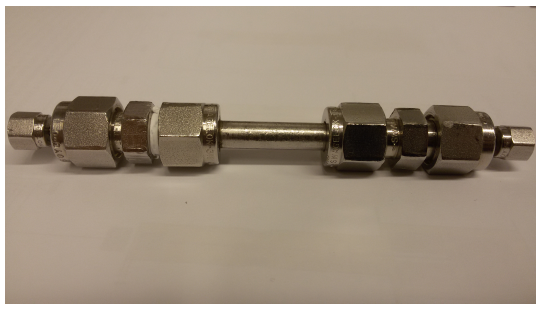

(b)

Figure 3.5: (a) Apparatus used for the pressure/depressurization test unit; (b) Column used for the tests.

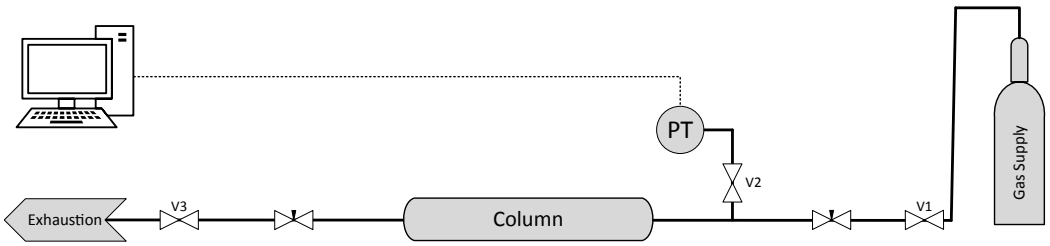

Figure 3.6: Schematic diagram of the pressure test unit. PT and V denote pressure transducer and valves respectively.

3.2.1.2 Abrasion Tests

A ballmill type aparatus, was used to obtain information about the mechanical resistance of the shaped MOF under high attrition conditions [65]. The ballmill (ULTRA-TURRAX®Tube Drive control, IKA) was used with steel balls with a diameter of 1.4cm and with a velocity of 400rpm for 2 minutes (Figure 3.7. Each sample was weighed before each test. After each test the sample was sieved between 1mm and 2mm in order to define the percentage of material that was damaged during the test.

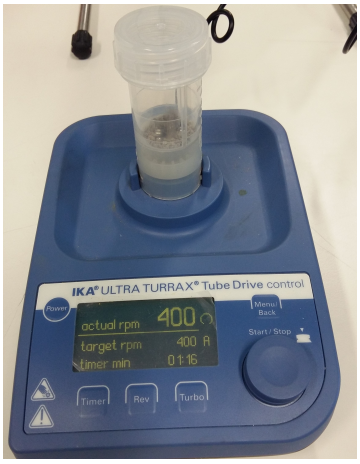

Figure 3.7: Ballmill apparatus used in the abrasion tests.

3.2.1.3 Drop Tests

A drop test apparatus, was used to obtain information about the mechanical resistance of the dried shaped MOFs during handling [65]. This method was only used on the shaped MIL-53(Al) samples with binder. The drop test was performed using a metal base where the samples were dropped from a height of 0.5m as shown in Figure 3.8. From each batch 20 pellets were dropped repeatedly from the same height and the number of drops until the sample broke was registered.

Figure 3.8: Drop Test Apparatus.

3.2.2 Structural and Physico-chemical Characterization of Samples

3.2.2.1 X-Ray Diffraction (XRD)

X-Ray diffraction (XRD) analysis was performed to evaluate the crystallinity of the MIL-53(Al) powder and of the binderless samples of MIL-53(Al) obtained. This analysis is obtained by studying the XRD peak positions. The main advantage of this method is that its a non-destructive method [72].

These analysis were performed in a X-Ray Diffractometer (XRD, Rigaku MiniFlex™ II) operating at room temperature. The radiation source was the Cu Kα line (λ = 1.5418Å) at a continuous scan at 0.5º (2θ) per minute over the range of 5º $\leq 2\theta \leq$ 50º, using a step of 0.02º (2θ) [44].

3.2.2.2 TGA

Thermogravimetric analysis (TGA) was performed to evaluate the samples weight loss while submited to increasing temperature. The extruded samples of MIL-53(Al)-PVA and also of only PVA were analysed by TGA (Model Q50 V6.7 Build 203, Universal V4.4, TA Instruments) under a nitrogen atmosphere at a heating rate of 10ºC/min up to 100ºC and kept at this temperature for 30 minutes and then heated at a rate of 5ºC/min up to 650ºC. Another analysis was performed with a initial heating rate of 10ºC/min up to 100ºC and kept at this temperature for 30 minutes and then heated at a rate of 10ºC/min up to 190ºC and then kept at this temperature for up to 24hours.

3.2.2.3 He Pycnometry

Helium pycnometry determines the volume occupied by the sample by actually measuring the pressure of helium in a calibrated volume. This method was used in order to

specify the skeletal density of the binderless samples. Before performing the analysis the samples were evacuated overnight at 200ºC. Helium intrusion was then measured at 35ºC in an automated gas displacement pycnometer (Accupyc 1330, Micromeritics).

3.2.3 Adsorption Equilibria

To measure the adsorption equilibrium of CO_2 at 30ºC of each sample the volumetric/-manometric method was used. The adsorption equilibrium measurements were obtained by using the volumetric unit shown in Figure 3.9 represented in the schematic diagram (Figure 3.10). This unit and its software were developed previously in-house [67] [73]. With this apparatus it is possible to measure simultaneously two different samples in parallel and the degassing is done in situ, since the cells used to contain the samples are placed inside of an oven with temperature control and both lines are also connected to a vacuum pump.

(a)

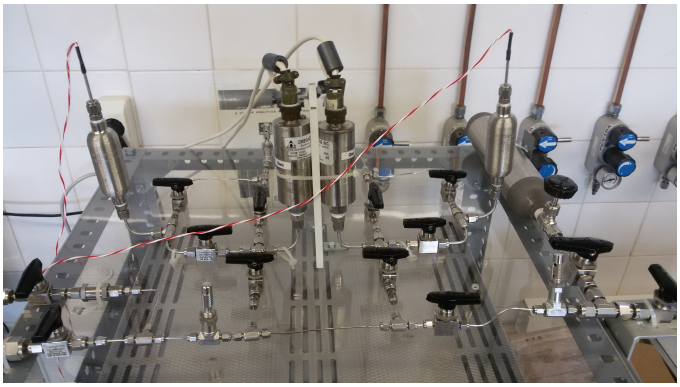

(b)

Figure 3.9: (a) General view of the volumetric unit.; (b) Detailed view of the main tubing and valves of the volumetric unit.

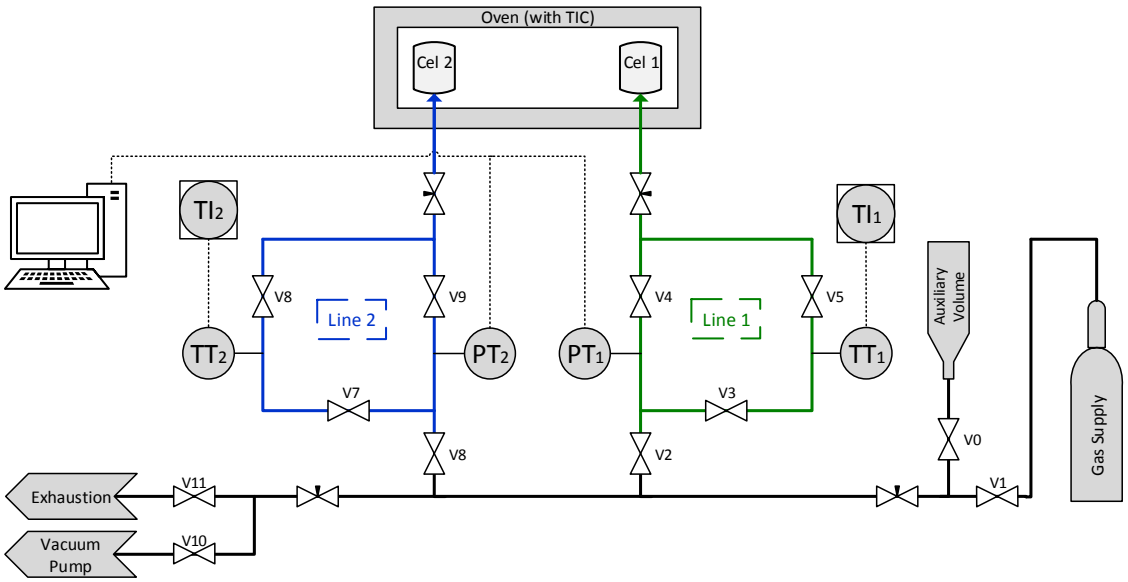

Figure 3.10: Schematic diagram of volumetric unit. The green section represents line 1; the blue section represents line 2; PT, TT and TI denote pressure transducers, temperature sensor and temperature indicator respectively; V represents the valves.

3.2.3.1 Calibration of the Volumetric Adsorption Unit

In order to use this unit for gas adsorption equilibrium measurements it is necessary to calibrate the sensors and the volumes. It is also important to refer that before proceeding with any measurement it is always necessary to ensure there are no leaks. The pressure transducers (PT) were calibrated using the manufactures guidelines (Omega Eng. Inc, USA) by checking the acquired voltages at atmospheric pressure and vacuum. The reference volumes ($Vref$) and the cell volumes ($Vcell$) must also be known.

The reference volumes $Vref_1$ and $Vref_2$ refer to the reference volumes of line 1 (green area in Figure 3.10) and line 2 (blue area in Figure 3.10), respectively. $Vref_1$ is the volume contained between valves V2, V4 and V5 (with V3 open). $Vref_2$ is the volume contained between valves V6, V8 and V9 (with V7 open). These volumes were calculated with aid of an auxiliary volume and were previously reported [73].

The calibration of the cells was necessary due to the fact that new cells were designed and built for the unit (Figure 3.11).

The cell volumes $Vcell_1$ and $Vcell_2$ are the cell volumes of line 1 and line 2, respectively. $Vcell_1$ is the volume between V4, V5 and the interior volume of $Cell_1$ and $Vcell_2$ is the volume between V8, V9 and the interior volume of $Cell_2$. A more detailed description of the calibrations is described in the Appendix A.4. This calibration was obtained by using helium (He) gas provided by Praxair (Portugal) with a purity of 99.999%. The gas densities were retrieved from the NIST Standard Reference Database [74]. The average references volumes, cell volumes and respective calculated errors of the unit are shown in Table 3.6.

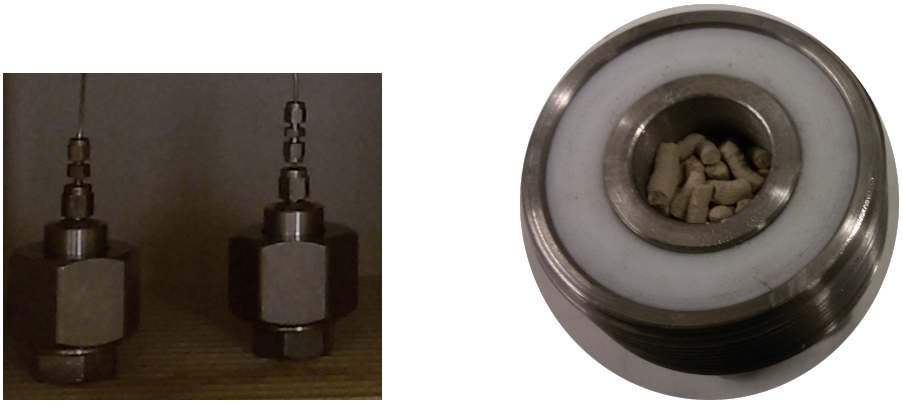

(a) (b)

Figure 3.11: (a) New cells used in the volumetric unit.; (b) Example of a cell with shaped MIL-53(Al) inside.

Table 3.6: Reference and cell volumes of the volumetic unit.

	Line 1	**Line 2**
Vref (cm^3)	41.54 ±0.03	41.51 ±0.03
Vcell (cm^3)	6.32 ±0.03	6.46 ±0.03

3.2.3.2 Measurements of Adsorption Equilibria

After the calibration of the volumetric unit, conditions are set to start measuring the isothermal adsorption equilibrium on the prepared samples. The adsorption equilibria measurements were carried out in the volumetric unit as shown in Figure 3.10. Each sample was tested in either one of the unit cells (Cell 1 or Cell 2) and the quantities of adsorbent were previously weighed. Before proceeding with the equilibria measurements, leaks were once more checked by using He gas, since it is an inert gas. Afterwards, the adsorbate used was CO_2 provided by Air Liquid (Portugal) with a purity of 99.998%. All the gas densities obtained for the measurements were retrieved from the NIST Standard Reference Database [74].

The first step for the adsorption equilibria measurements is to degas the adsorbents. To degas the samples they were heated "in situ" at a rate of 2ºC/min up to 200ºC or 190ºC, for the binderless samples or for the samples with binder respectively, and maintained at these temperatures for 3 hours under vacuum. Afterwards, the temperature during the measurements was maintained at 30ºC. Carbon dioxide adsorption equilibria for the various samples were carried out with the same protocol, as described in Appendix A.5.

To report adsorption equilibrium measurements different methods are used, one is the net adsorption (q_{net}), which is calculated from total amount of gas present in the cell that contains the adsorbent, minus the amount that would be in the empty cell (at the same pressure and temperature). However it is more common to report adsorption results as excess amount adsorbed (q_{ex}), which gives the number of molecules in the nanopores

of the adsorbent in excess of the amount that would be in found in the pore volume. Absolute adsorption (q) is another alternative to present equilibrium measurment results and relates three adsorption quantities: net, excess and absolute, but for these last two it is necessary to know the skeletal density and the specific pore volume of the adsorbent used [16]. Therefore, since the skeletal density and specific pore volume was not obtained for all of the samples the adsorption equilibrium measurements for this study are reported as q_{net}.

To calculate the net amount adsorbed at equilibrium, equations 3.3 and 3.4 are applied where: m_{net} is the net adsorbed mass at equilibrium (g); ρ_{ref} and ρ_{cell} are the gas densities in the reference volume and in the cell volume respectively (g/cm^3); $Vcell$ is the volume of the cell (cm^3); q_{net} is the net amount adsorbed per unit of adsorbent (mol/kg); m_s is the adsorbent mass (g); and $M(CO_2)$ is the carbon dioxide molar mass (g/mol).

$$m_{net_n} = m_{net_{n-1}} + [(\rho_{ref,i_n} - \rho_{ref,f_n})V_{ref} + (\rho_{cell_{n-1}} - \rho_{cell_n})V_{cell}] \tag{3.3}$$

$$q_{net_n} = \frac{m_{net_n}}{m_s \times M(CO_2)} \times 1000 \tag{3.4}$$

Chapter 4

Experimental Results and Discussion

This chapter presents the results and analysis of the experimental work performed. Two different methods were used to shape the MOF MIL-53(Al) powder: binderless (by mechanical compression) and with binder (by extrusion). Both methods and the results obtained are discussed and compared bellow. Several characterization analysis of the samples and their comparisons with the primary powdered material were performed. Mechanical characterization (pressure/depressurization, abrasion and drop tests), structural and physico-chemical characterization (XRD analysis, TGA and He pycnometry) and adsorption equilibrium measurements are reported.

4.1 Shaping MIL-53(Al)

4.1.1 Binderless Shaping

Two different samples were obtained using this method: one batch compressed at 1tf force and another compressed at 0.5tf. Both samples are visually identical (Figure 4.1). These forces were used for two reasons: i) when testing this method with activated carbon the pellets with more than 1tf compression were very brittle and fragile; ii) a previous study preformed with another MOF, ZIF-8, showed that with a compression of 0.5tf, the BET surface area of the MOF is completely preserved, with a compression of 1tf only 4.1% of the BET surface area is lost, while with forces above this range losses are above 10% in comparison to the powdered ZIF-8 [18].

The method employed was quite simple and reproducible in order to shape MIL-53(Al). As shown in figure 4.1, the shaped material has a random and granulated shape, with particle size in the range of 1-2mm. The main drawbacks of this method is its reproducibility (with the press used it is not easy to ensure that the force employed in the compression is the same in all the batches made), the time that is necessary to produce

a larger quantities of material and also the amount of waste of the adsorbent that is produced, since when crushing the pellets into smaller bodies, part of the material is crushed into very fine particles that can not be further used for this method.

Table 4.1: Binderless MIL-53(Al) Samples and Observations.

Batch	Force (tf)	Sieve (mm)	Observations
A1	1	1 - 2	Consistent particles with irregular shapes
A2	0.5	1 - 2	Consistent particles with irregular shapes

(a) (b)

Figure 4.1: MIL-53(Al) Binderless Samples: (a) Batch A1; (b) Batch A2.

4.1.2 Shaping with Binder

Mixtures with different PVA aqueous solutions and with distinct viscosities were prepared. Seven samples were obtained (Table 4.2), although only four showed potential (B1, B3, B5 and B7) from a mechanical point of view. These samples when extruded with the syringe into "spaghetti" like shape maintained their form and when dried were easy to break into smaller pellet like particles. Therefore batches B1, B3, B5 and B7 (Figure 4.3) were the binder containing samples that were selected for further study of their mechanical, physico-chemical and adsorptive characteristics. The other batches (B2, B4 and B6) resulted into very fluid mixtures that when extruded did not keep the desired shape. For this reason, these were set aside and no further characterizations were performed (Figure 4.2).

The main challenge of this method was to get the right mixture and viscosity to obtain an uniform extrudate. The composition of the mixtures can vary from material to material, for example the same method was applied with another MOF, namely ZIF-8, and using also PVA aqueous solutions as a binder, the obtained extrudates were not as uniform and easily obtained [75]. Therefore it can be concluded that although this method shows good results with MIL-53(Al) when applying to a different powder adjustments to the mixtures and methods might be necessary.

This method is relatively faster to obtain larger amounts of extrudates and there is less waste of the primary the powder compared to the binderless method. Handling the dried samples and cutting them into smaller extrudates showed that the samples with less percentage of binder (2% and 5%) were more fragile and more breakable than the samples with more binder (10% and 15%). The drawbacks in this method is its reproducibility, two batches with the same recipe might not be identical due to a number of factors, especially the human factor. When preparing the mixtures, as it is done manually, the mixture might not be always homogenized equally and during the extrusion the pressure used and the precision can vary. The extrudates obtained are not 100% uniform in size and shape, and more importantly when using a binder there is a compromise between the surface area of the adsorbent and the amount of binder employed.

Table 4.2: MIL-53(Al)-PVA Extruded Samples and Observations.

Batch	Binder (% w/w)	PVA Solution (Batch)	Observations
B1	2	**PVA2**	**Relatively uniform extrudate**
B2	5	PVA2	Resulting extrudate was not very uniform.
B3	**5**	**PVA5**	**Relatively uniform extrudate.**
B4	10	PVA5	Not possible obtain an extrudate.
B5	**10**	**PVA10**	**Relatively uniform extrudate.**
B6	15	PVA10	Resulting extrudate was not very uniform.
B7	**15**	**PVA15**	**Relatively uniform extrudate.**

Figure 4.2: Example of a batch (B4) that was not possible to extrudate into pellet like shapes.

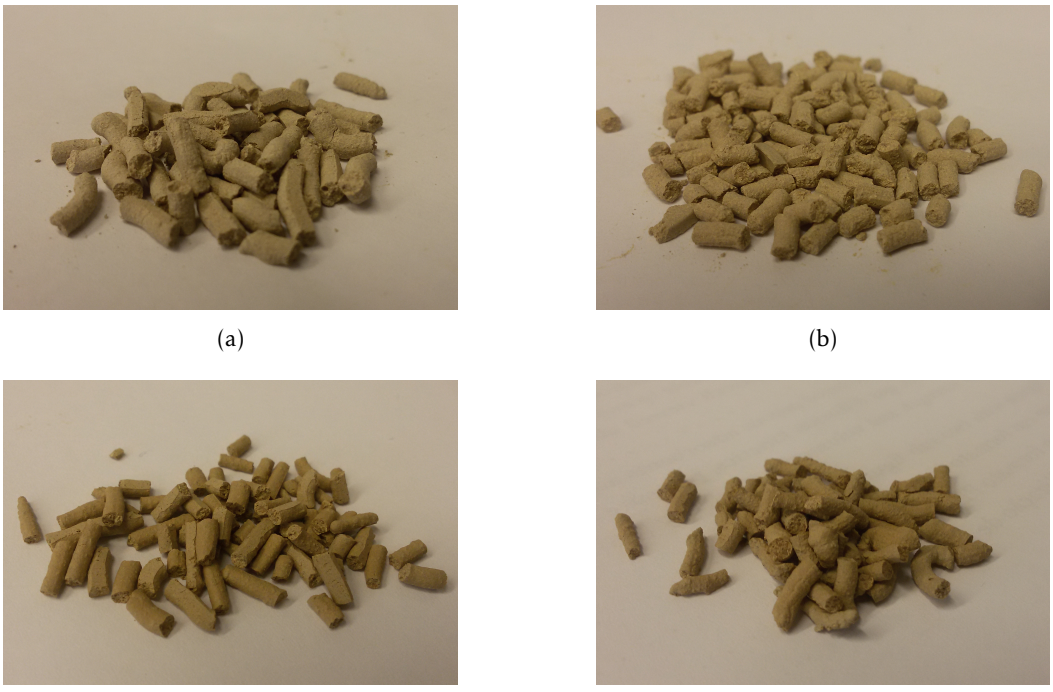

(a) (b)

(c) (d)

Figure 4.3: Selected MIL-53(Al)-PVA Dried Batches: (a) Batch B1 (with 2% PVA); (b) Batch B3 (with 5% PVA); (c) Batch B5 (with 10% PVA); (d) Batch B7 (with 15% PVA).

4.2 Characterization of Shaped MIL-53(Al)

4.2.1 Mechanical Characterization of Samples

4.2.1.1 Pressure/depressurization Tests

Pressure/depressurization tests were employed to simulate pressure changes upon the packed particles. This allows to understand the mechanical resistance of the shaped adsorbent particles under pressure cycles, thus simulating the operation of a packed adsorption column. This test must be viewed as a qualitative analysis that shows an estimate of the percentage of the mass of the sample lost during the pressure modulation cycles (in the case of the binderlessa samples). For the samples with binder, the number of pellets inserted into the column were counted and afterwards were counted again to check if any pellets was broken during the cycles.

The results obtained are in tables 4.3 and 4.4. We can conclude that sample A1 (with 1tf compression) overall shows greater loss of material during the different cycles than samples A2 (with 0.5tf compression). Also in the cycles that reach higher pressure (18bar) there is significantly a larger loss of material. Both binderlesss samples show a good mechanical resistance, since they lose less than 5% of mass and therefore potentially are suitable to be used in adsorption-based applications.

In the case of the binder containing samples no loss was registered with samples B5

(with 10% PVA) and B7 (with 15% PVA), which shows a good mechanical resistance and is in good agreement with the quantity of binder in the samples. The only samples which show less mechanical resistance is sample B3 (with 5% PVA) and B1 (with 2% PVA). The sample with less binder shows the least resistance and might reveal to not be suitable to use in adsorption-based applications from a mechanical point of view.

Table 4.3: Pressure/Depressurization Test Results of Binderless Samples

Sample	Cycle (bar)	Initial Weight (g)	Final Weight (g)	% Mass Loss
A1	3	0.2813	0.2769	1.6
	10	0.3094	0.3025	2.2
	18	0.2982	0.2856	4.2
A2	3	0.2591	0.2575	0.6
	10	0.3155	0.3122	1.0
	18	0.3367	0.3267	3.0

Table 4.4: Pressure/Depressurization Test Results of Samples with Binder

Sample	Cycle (bar)	Initial No. Pellets	Final No. Pellets	% Lost
B1	3	16	16	0.0
	10	16	15	6.3
	18	16	14	12.5
B3	3	16	16	0.0
	10	16	15	6.2
	18	16	16	0.0
B5	3	16	16	0.0
	10	16	16	0.0
	18	16	16	0.0
B7	3	16	16	0.0
	10	16	16	0.0
	18	16	16	0.0

4.2.1.2 Abrasion Tests

The abrasion test verifies the mechanical resistance of the shaped MOF under abrasion. This method showed to be quite aggressive and destructive and was only performed on the binderless samples. The results obtained are shown in table 4.5, where sample A1 (with 1tf compression) lost approximately 30% of its initial weight and sample A2 (with 0.5tf compression) lost approximately 46% of its initial weight. This qualitative test shows that sample A1 has better mechanical resistance under abrasion when compared with sample A2. This method is quite aggressive and does not simulate accurately the

conditions that these materials undergo in an adsorption-based processes, therefore no further conclusions can be obtained.

Table 4.5: Abrasion Test Results

Sample	Initial Weight (g)	Final Weight (g)	% Lost
A1	0.9965	0.7016	30
A2	0.9846	0.5278	46

4.2.1.3 Drop Tests

A Drop Test apparatus, was used to obtain information about the mechanical resistance of the MIL-53(Al) shaped particles during their handling. This test was only performed on the binder containing samples. The results obtained are summarized in table 4.6, where the samples with less percentage of binder showed less resistance, as expected. In the particular case of sample B7 with 15% of PVA, over 30 drops were performed on samples and no breaking was observed, which shows that this sample is the most resistant, as it would be expected. The results obtained from these tests are viewed as qualitative only, a complete table with all of the drop tests performed, along with the calculated average and associated error, are shown in the Appendix A.1 (Table A.1).

Table 4.6: Drop Test Results

Sample	Average Number of Drops	Error
B1	3.75	1.92
B3	5.50	1.82
B5	7.40	1.96
B7	>30	not applicable

4.2.2 Structural and Physico-chemical Characterization of Samples

4.2.2.1 X-Ray Diffraction (XRD)

X-Ray diffraction (XRD) analysis performed on MIL-53(Al) powder and on binderless samples A1 and A2 evaluate their crystallinity. Figure 4.4 shows the XRD patterns which can provide a qualitative comparison between the samples. Comparing these results with other previous studies of XRD analysis of compressed MOFs it was unexpected to see this significant change between the powder and the compressed samples. XRD results of CuBTC and of ZIF-8 show that at similar compressions no significant alteration in the crystallinity was observed [18, 57, 75]. These significant differences in the patterns suggest possible modification of the crystalline properties between the binderless samples and their respective powder. The most predominant peak in the powdered sample appears at

2θ=8.79º (Figure A.1), while in samples A1 and A2 the higher peak appears at 2θ=26.93 and 2θ=26.75, respectively (see Appendix A.2 Figures A.2 and A.3). Furthermore, the XRD powder diffraction pattern of the powder sample was indexed as monoclinic with the spacegroup Cc, using the software Expo2014 [76]. The unit cell parameters obtained for the MIL-53(Al) in its primary powder form are shown in Appendix (Table A.2) which are in good agreement with other results previously reported [40, 44, 77, 78].

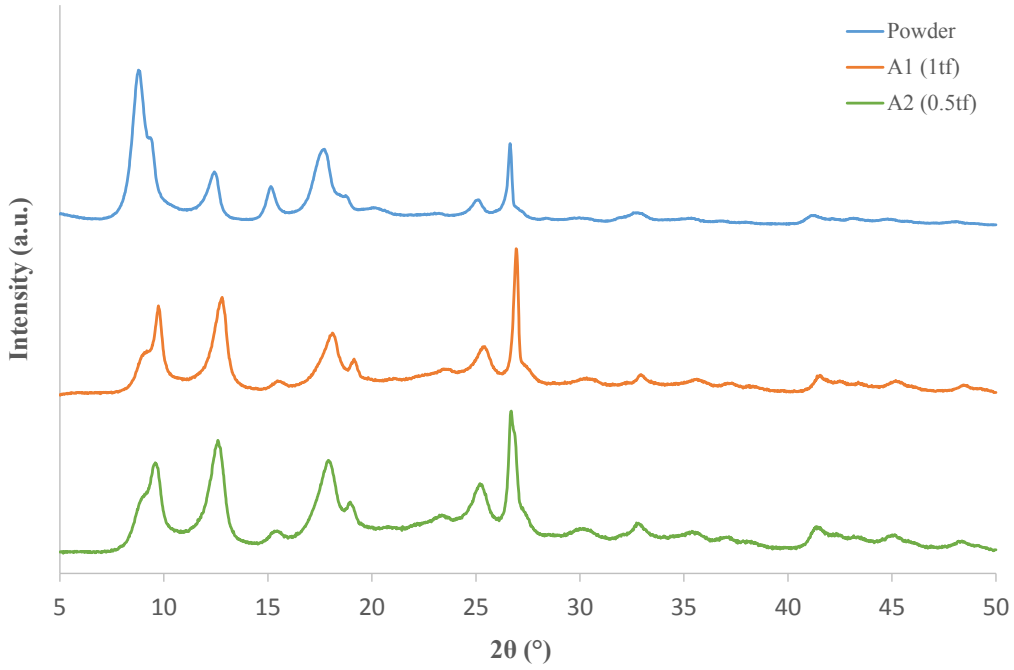

Figure 4.4: Experimental XRD paterns of MIL-53(Al) powder and binderless samples A1 and A2.

4.2.2.2 Thermogravimetric analysis

Thermogravimetric analysis (TGA) were performed on the primary MIL-53(Al) powder and on the samples with binder (B1 with 2% PVA, B3 with 5% PVA, B5 with 10% PVA and B7 with 15% PVA). Each batch were analysed two times with different time and temperature conditions and are shown individually in the appendix in more detail (see Appendix A.3). In Figure 4.5 are shown 4 different samples and their weight loss (%) as a function of the temperature (K). All the samples show significant stability up to 450K; above this temperature they show gradual mass loss and above 750K a more accentuated degradation is observed. The samples with higher percentage of PVA (B5 and B7) show a more significant weight loss compared to samples with less amount of binder (B1 and B3).

As the degassing temperature for the adsorption equilibrium experiments will be at 463K in figure 4.6 the same TGA graph is shown for the 4 samples but with more detail between 300K and 460K. At 463K samples B1, B3, B5 and B7 lose 3.45%, 4.52%,

5.85% and 5.22% of mass weight respectively (see Appendix A.3 Figures A.4, A.5, A.6, A.7). These weight losses were applied to calculate the weight of adsorbent used in the adsorption equilibrium experiments after degassing, since the manometric system only permits to weigh the mass of the samples prior to its "in situ" degassing.

Sample B1 and B2 show a weight loss slightly above a 2% weight loss previously reported for MIL-53(Al) in its primary powder form [44]. Samples B7 with 15% of PVA surprisingly shows a lower weight loss at this temperature compared to sample B5 with 10% PVA but the difference is not significant. Furthermore, the samples were also tested with TGA at a constant temperature for at least 2.5hours at 463K where in no sample more than 6% weight loss was registered (see Appendix A.3 Figures A.8, A.9, A.10, A.11).

TGA was also performed on the pure PVA used as a binder. The manufacturer stated that the melting point of PVA (Mowiol® 10-98) was at 473K [71]. In Figure 4.7 we can see that up to 473.15K no significant weight loss is observed and at this temperature only 1.95% of its weight is lost.

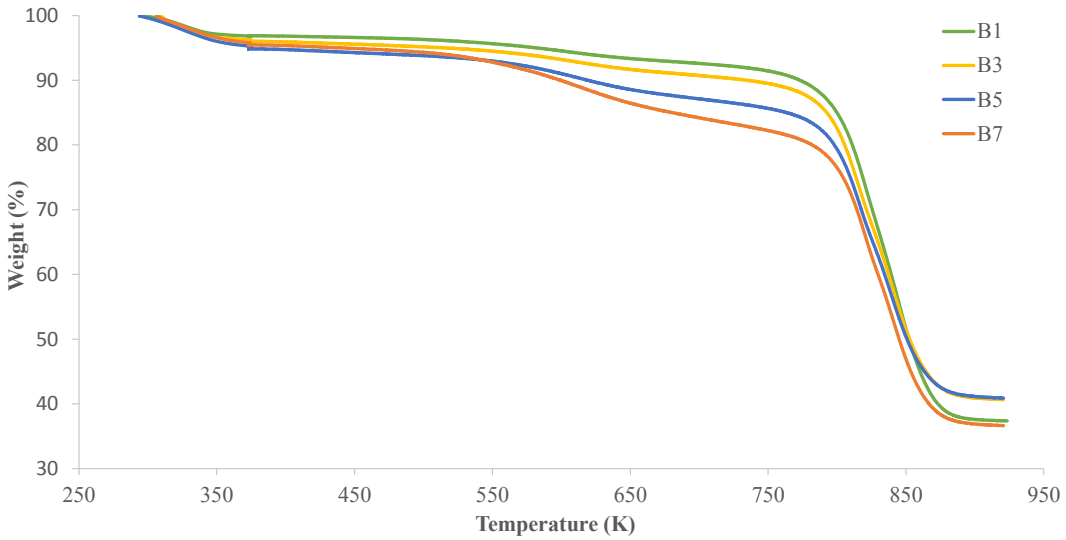

Figure 4.5: TGA of samples B1 (with 2% binder), B3 (with 5% binder), B5 (with 10% binder) and B7 (with 15% binder).

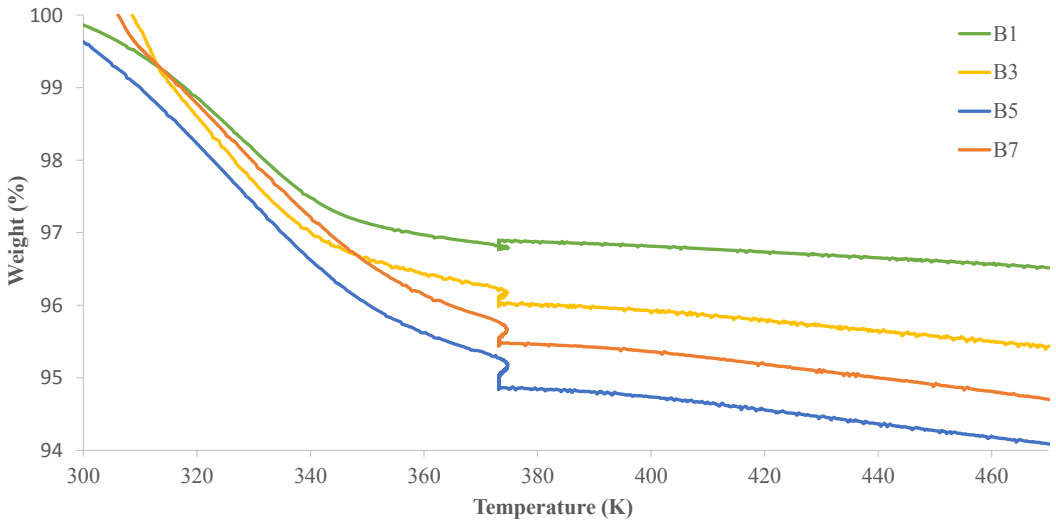

Figure 4.6: TGA of samples B1 (with 2% binder), B3 (with 5% binder), B5 (with 10% binder) and B7 (with 15% binder) between 300K and 460K.

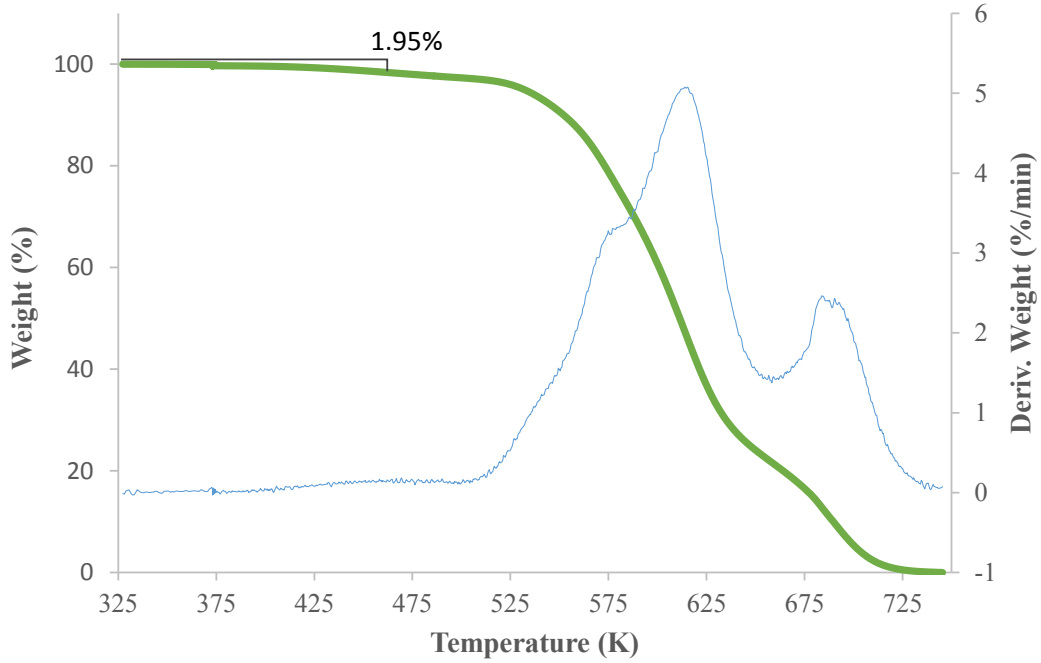

Figure 4.7: TGA of pure PVA (Mowiol® 10-98).

4.2.2.3 Helium Pycnometry

Helium pycnometry results for the binderless samples are shown in Table 4.7. Here it can be concluded that no significant alteration in the skeletal density of the shaped materials is registered from the powder form to the compressed samples A1 and A2.

Table 4.7: He Pycnometry Results for the Binderless Samples and MIL-53(Al) powder.

Sample	**Density** (g/cm^3)
Powder	1.60
A1	1.61
A2	1.61

4.2.3 Adsorption Equilibrium Experiments

Adsorption equilibria measurements of CO_2 on the MIL-53(Al) shaped samples were performed in the volumetric unit at 30ºC temperature from 0 to 20 bar pressure range. The results were compared with previous adsorption equilibria measurements of MIL-53(Al) in its powder form [16].

Adsorption isotherms were measured to examine the adsorption and desorption capacity for CO_2 of the different shaped samples. The binderless samples and the samples with binder are first analysed separately and finally a global analysis of all the samples is discussed.

In Figure 4.8 the two CO_2 sorption isotherms of the binderless samples A1 and A2 (compressed at 1tf and 0.5tf respectively) are represented and compared with the isotherm obtained for MIL-53(Al) in its primary powder form. Although these compressed samples are composed of 100% MIL-53(Al) and no binder is associated to these pellets there is a significant decrease in CO_2 loading per mass of adsorbent compared to the powder. This decrease may be associated with modifications in the crystal structure due to the compression of the powder as suggested by the XRD results. Sample A2, which was compressed at a lower pressure shows a higher adsorption capacity of CO_2 when compared to sample A1.

The CO_2 adsorption of both samples up to a pressure approximately of 4bar show no significant decrease in adsorptin compared to the powder in the same conditions. Above a pressure of 4bar, sample A2 losses globally approximately 20% of the CO_2 adsorption capacity compared to the powder form, while sample A1 shows approximately 35% less. Moreover the CO_2 adsorption isotherms show an expected Langumir type isotherm (Type I by IUPAC). The desorption branches in both samples show some hysteresis, following the trend of the original powder. However the solids are completely regenerated suggesting that the adsorbents are totally reversible concerning the adsorption of CO_2.

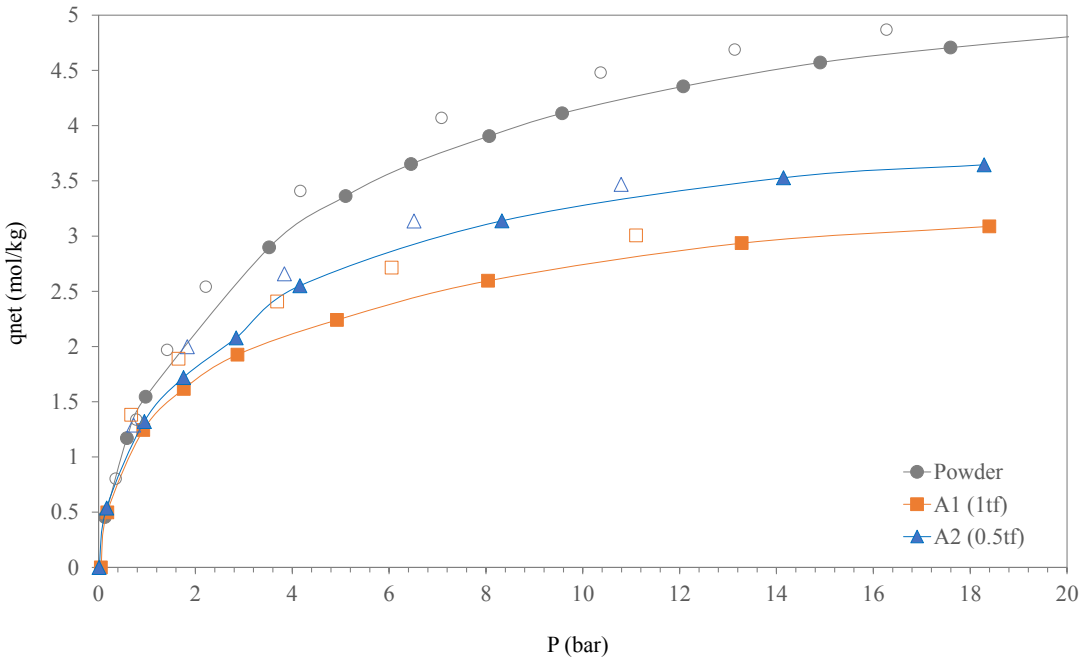

Figure 4.8: Net adsorption equilibrium isotherms of CO_2 at 30ºC on the MIL-53(Al) powder, sample A1 (binderless MIL-53(Al) pellets compressed at 1tf) and sample A2 (binderless MIL-53(Al) pellets compressed at 0.5tf). Closed symbols denote adsorption data and open symbols denote desorption data. Lines are drawn as a guide to the eye.

The CO_2 adsorption equilibria on the shaped samples suggest that a mechanical compression larger than 0.5tf compromises significantly the adsorption capacity of MIL-53(Al). Furthermore, granulates with 0.5tf compression show more promising results and may be envisioned for application in future studies for gas adsorption separation.

Previously CO_2 isotherms for compressed MOF have been reported. For the CuBTC about 50% of adsorption capacity is lost although a much higher compression force was used, while for ZIF-8 at a similar 0.5tf compression almost no loss in CO_2 adsorption capacity was observed [63, 75].

Figures 4.9 and 4.10 represent the CO_2 adsorption equilibrium isotherms (30ºC) over the four MIL-53(Al) binder containing samples and the primary powder form. Since all of these samples present a percentage of binder (from 2% to 15%), it is expected a decrease in the CO_2 sorption capacity may occur. The binder decreases the effective surface area and can also block pores, reducing the available pore volume of the adsorbent particles. Effectively all the samples show a decrease in the CO_2 loading capacity and with larger percentages of binder a more significant decrease is observed. All the samples show Langumir type isotherms (Type I by IUPAC) and no significant hysteresis is observed.

Samples B1 and B3, with 2% and 5% binder respectively, show greater CO_2 adsorption capacity compared with samples B5 and B7, with 10% and 15% binder respectively. Overall samples B1 and B3 show a similar adsorption capacity, and above the pressure of

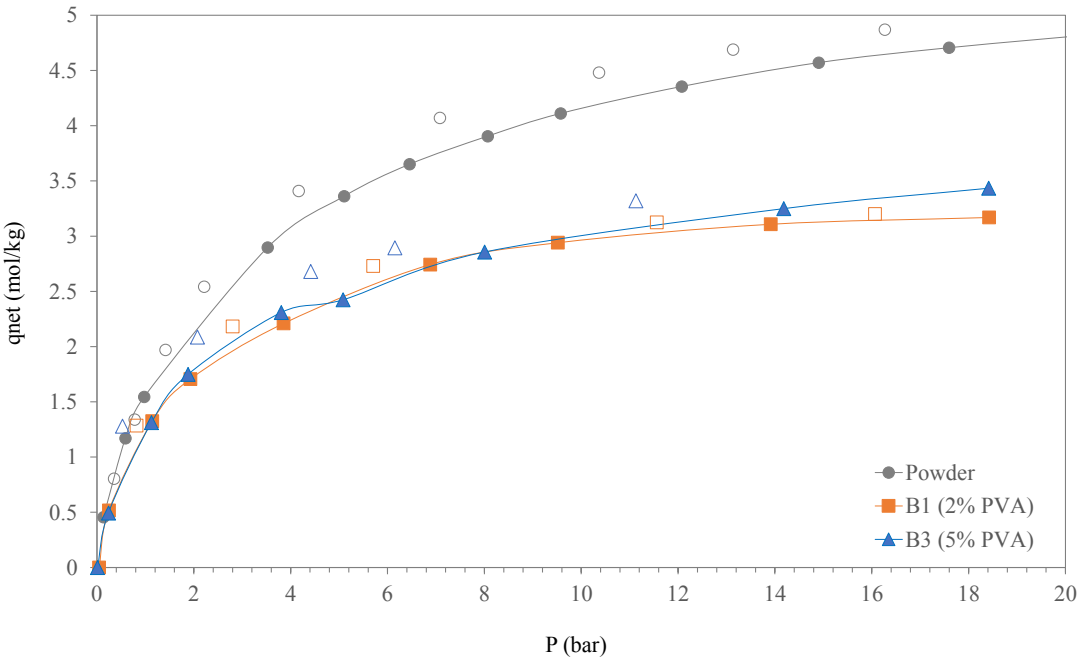

Figure 4.9: Net adsorption equilibrium isotherms of CO_2 at 30°C on the MIL-53(Al) powder, sample B1 (MIL-53(Al) with 2% PVA binder) and sample B3 (MIL-53(Al) with 5% PVA binder). Closed symbols denote adsorption data and open symbols denote desorption data. Lines are drawn as a guide to the eye.

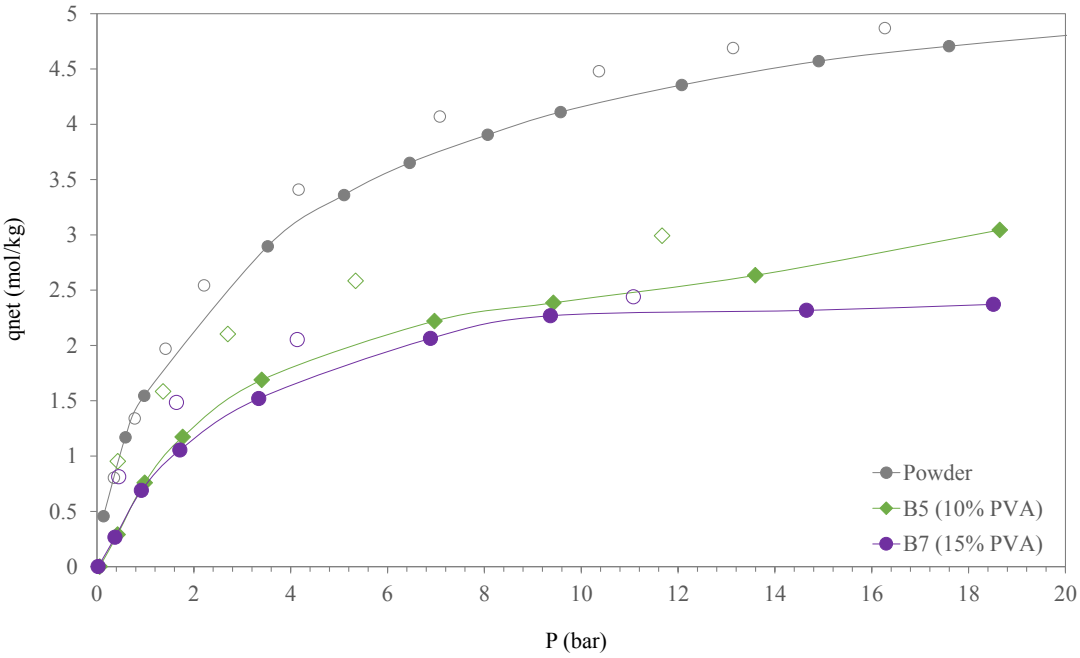

Figure 4.10: Net adsorption equilibrium isotherms of CO_2 at 30°C on the MIL-53(Al) powder, sample B5 (MIL-53(Al) with 10% PVA binder) and sample B7 (MIL-53(Al) with 15% PVA binder). Closed symbols denote adsorption data and open symbols denote desorption data. Lines are drawn as a guide to the eye.

4 bar they both show an average 30% less adsorption capacity compared to the powder. However sample B3 has a greater percentage of binder in comparison with sample B1 and shows a slightly higher adsorption capacity, which is unexpected. Hence as both samples have very small percentages of PVA binder a number of factors might be responsible for this difference. One possible explanation is that during the mixture of sample B1 the PVA caused more blockage of the pores of MIL-53(Al) or that during the degassing of the sample a greater degradation was presented then proposed by the TGA analysis. These results suggest that more samples should be prepared and further adsorption equilibrium experiments should be performed to validate the results.

Previously CO_2 isotherms for MOFs with PVA binder have been reported. For UTSA-16 the adsorption isotherms for CO2 at 25ºC different PVA percentages were studied from 0.7% to 6.7%, where the sample with 2% PVA shows a very small adsorption capacity loss compared to its primary powder, while at 6.7% a maximum of 25% of adsorption loss is observed [59]. These results show that although it was expected to see a better performance of sample B1 (with 2% PVA binder), sample B3 (with 5% PVA) shows an expected CO_2 capacity loss.

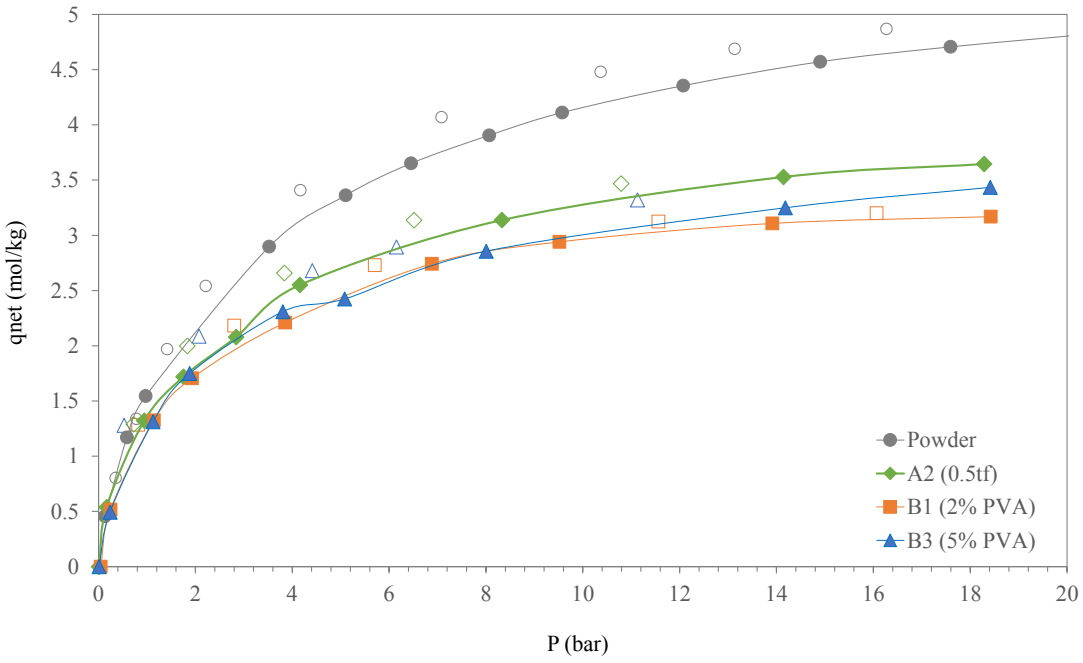

Figure 4.11: Net adsorption equilibrium isotherms of CO_2 at 30ºC on the MIL-53(Al) powder, sample A2 (binderless MIL-53(Al) pellets compressed at 0.5tf), sample B1 (MIL-53(Al) with 2% PVA binder) and sample B3 (MIL-53(Al) with 5% PVA binder). Closed symbols denote adsorption data and open symbols denote desorption data. Lines are drawn as a guide to the eye.

Sample B5 and sample B7 above a pressure of 4bar show approximately 40% and 45% less adsorption capacity respectively compared with powder. This loss is significant and show that adding more than 10% of PVA binder to MIL-53(Al) compromises the CO_2

adsorption capacity of this binder containing shaped MOF.

In summary the binderless sample A1 (compressed at 0.5tf) shows the best CO_2 adsorption capacity from all of the six samples tested in the volumetric unit, followed by the samples with PVA binder, sample B3 (with 5% PVA binder) and B1 (with 2% PVA binder). In figure 4.11 the three CO_2 isotherms at 30ºC with best results are presented. These show the most promising results in the shaping of MIL-53(Al) for adsorption based processes.

Chapter 5

Conclusions and Future Work

This chapter summarizes the work done in this dissertation in order to achieve its objectives. Furthermore, it discusses potential future work that may enhance the work done in this dissertation. This work focused on two main objectives: shaping MIL-53(Al) with two different methods (binderless and with binder) and characterize the obtained shaped materials.

5.1 Conclusions

In this work MIL-53(Al) was shaped using two distinct methods. One method used was a binderless technique, where MIl-53(Al) powder was shaped by compression, using a pellet press at two different forces (0.5ton compression and 1ton compression). Alternatively, MIL-53(Al) was also shaped using a binder, in this case a PVA solution was mixed with the MOF in different percentages (2%, 5%, 10% and 15%) and extruded into pellet like shaped bodies. Technically both methods were successful in shaping MIL-53(Al).

Once the different samples were shaped mechanical characterizations were performed on the materials in order to assess if the obtained shaped particles had a good mechanical resistance and thus showing potential for application in scale up processes. Results obtained showed that no significant difference was observed between the two binderless samples. The samples with binder showed significant differences between each other, where the samples with less percentage of binder (2% and 5%) show significantly less mechanical resistance when compared with the samples with higher percentages of binder (10% and 15%).

Several physico-chemical characterizations were performed on the samples: XRD, TGA and He pycnometry analysis. The XRD analysis were performed on the binderless

samples, where it was observed significant differences in the patterns that suggest possible modification of the crystalline properties between the binderless samples and their respective powder. TGA analysis were performed on the samples with binder where it was observed globally that with higher percentages of PVA binder there is a higher weight loss. He pycnometry was performed on the binderless samples and show that with compression no significant alteration is observed in the skeletal densities between the compressed samples and the primary powder.

Adsorption equilibria of the CO_2 on the MIL-53(Al) shaped samples were performed in a volumetric unit at 30ºC temperature from 0 to 20 bar pressure range. The results were compared with previous adsorption equilibria measurements of MIL-53(Al) in its powder form. The shaped MIL-53(Al) particles all showed a decrease of adsorption in comparison with MIL-53(Al) in its powder from. However, of the six shaped samples, only three showed overall a greater potential in CO_2 adsorption capacity. The sample with the highest adsorption capacity was shaped using the binderless method with a compression of 0.5ton, with approximately 20% adsorption capacity loss in comparison with the powder (above a pressure of 4bar). The other two samples with high adsorption capacities were the samples containing binder with 2% and 5% PVA percentages, where both show similar adsorption capacities, but it is observed at least 30% less adsorption capacity (above a 4bar pressure) compared to the powder.

This study suggests that both shaping methods may be valid for further application in gas adsorption processes. The binderless method shows most promise with its CO_2 adsorption capacity and mechanically these particles show a good resistance, but the patterns observed in the XRD analysis of this material suggest that this may have suffered possible modifications in the crystalline properties. Therefore, it is possible that if a lower compression had been employed to shape MIL-53(Al) (with the binderless method), an even higher adsorption capacity would had have been observed. The samples with 2% binder and 5% binder both show similar CO_2 adsorption capacity, although there are mechanical and physico-chemical differences between the two samples. The results from the mechanical resistance test suggest that the sample with 5% binder has a better mechanical resistance, while the TGA analysis shows that with more binder a greater degradation of the material is observed. Overall both binderless samples show potential, and results suggest that adding up to a 5% of PVA as a binding agent for MIL-53(Al) is the best approach for this type of shaping method targeted for gas adsorption processes.

5.2 Future Work

Despite the significant work developed for this dissertation, that allowed a better understanding in how to shape the MOF MIL-53(Al) for gas adsorption processes, there is still work to be developed regarding the physico-chemical characterizations.

Due to time limitations is was not possible to obtain nitrogen (N_2) adsorption isotherms at 77K or mercury (Hg) porosimetry for any of the samples studied in this work, which are

essential to fully evaluate the characteristics and applicability of these shaped materials in gas adsorption processes. Also XRD analysis, Helium pycnometry were only performed on the binderless samples and should be conducted on the samples with binder. Thermogravimetric analysis (TGA) was also not performed on the binderless MIL-53(Al) samples. Afterwards completed all of the remaining analysis of the shaped materials developed in this work, there are other recommendations for future work in this field:

- The CO_2 adsorption equilibrium measurements should be repeated with similar samples in order to assess reproducibility of these results. Furthermore more samples with binder could be developed and tested in the same conditions with a percentage of PVA binder ranging between 2% and 5%. Using the binderless method a compression force lower than 0.5tf could also be tested using another hydraulic press for example.
- The more suitable samples obtained in this dissertation may be selected for a scale-up production, thus being applied in lab-scale fixed-bed adsorption columns in order to evaluate their behaviour under dynamic conditions.
- Other MOFs should be shaped and studied, as it is clear that with different adsorbents the shaping method may vary. Furthermore novel shaping techniques should be tested on MOFs, such as 3D printing that may allow to create more complex and defined shaped particles.

Bibliography

[1] UNFCCC. Conference of the Parties (COP). *Adoption of the Paris Agreement. Proposal by the President*. Geneva, 2015. URL: http://unfccc.int/resource/docs/2015/cop21/eng/l09r01.pdf.

[2] European Environment Agency. *Climate agreement: towards a low-carbon, climate resilient world*. Tech. rep. Copenhagen, 2015, p. 6. URL: http://www.eea.europa.eu/articles/climate-agreement-towards-a-low.

[3] IPCC. *Climate Change 2014: Mitigation of Climate Change. Working Group III Contribution to the Fifth Assessment Report of the Intergovernmental Panel on Climate Chang*. Ed. by O. Edenhofer, R. Pichs-Madruga, Y. Sokona, J. C. Minx, E. Farahani, S. Kadner, K. Seyboth, A. Adler, I. Baum, S. Brunner, P. Eickemeier, B. Kriemann, J. Savolainen, S. Schlömer, C. von Stechow, and T. Zwickel. Cambridge, United Kingdom and New York, NY, USA: Cambridge University Press, 2014. ISBN: 9781107654815. URL: http://www.ipcc.ch/report/ar5/wg3/.

[4] EEA. *The european environment - state and outlook 2015: synthesis report*. Copenhagen: European Environment Agency, 2015. DOI: 10.2800/944899.

[5] ICAP. *Emissions Trading Worldwide: Status Report 2016*. Tech. rep. Berlin: ICAP, 2016. URL: https://icapcarbonaction.com/en/status-report-2016.

[6] European Environment Agency. *Climate change : investing in low-carbon solutions and adaptation*. Tech. rep. Copenhagen, 2014, p. 7. URL: http://www.eea.europa.eu/articles/climate-change-investing-in-low.

[7] L. Espinal, D. L. Poster, W. Wong-Ng, A. J. Allen, and M. L. Green. "Measurement, Standards, and Data Needs for CO 2 Capture Materials: A Critical Review". In: *Environmental Science & Technology* 47.21 (2013), pp. 11960–11975. ISSN: 0013-936X. DOI: 10.1021/es402622q.

[8] OECD/IEA. *World Energy Outlook 2015*. World Energy Outlook. Paris: OECD Publishing, 2015, p. 200. DOI: 10.1787/weo-2015-en.

[9] M. K. Mondal, H. K. Balsora, and P. Varshney. "Progress and trends in CO2 capture/separation technologies: A review". In: *Energy* 46.1 (2012), pp. 431–441. ISSN: 03605442. DOI: 10.1016/j.energy.2012.08.006.

[10] EEA. *Air pollution impacts from carbon capture and storage (CCS)*. Tech. rep. Technical Report 14/2011. Copenhagen: European Environment Agency, 2011, p. 66. DOI: 10.2800/84208.

[11] J.-R. Li, Y. Ma, M. C. McCarthy, J. Sculley, J. Yu, H.-K. Jeong, P. B. Balbuena, and H.-C. Zhou. "Carbon dioxide capture-related gas adsorption and separation in metal-organic frameworks". In: *Coordination Chemistry Reviews* 255.15-16 (2011), pp. 1791–1823. ISSN: 00108545. DOI: 10.1016/j.ccr.2011.02.012.

[12] A. A. Olajire. "CO2 capture and separation technologies for end-of-pipe applications – A review". In: *Energy* 35.6 (2010), pp. 2610–2628. ISSN: 03605442. DOI: 10.1016/j.energy.2010.02.030.

[13] Y. Liu, Q. Ye, M. Shen, J. Shi, J. Chen, H. Pan, and Y. Shi. "Carbon Dioxide Capture by Functionalized Solid Amine Sorbents with Simulated Flue Gas Conditions". In: *Environmental Science & Technology* 45.13 (2011), pp. 5710–5716. ISSN: 0013-936X. DOI: 10.1021/es200619j.

[14] S. Choi, J. H. Drese, and C. W. Jones. "Adsorbent Materials for Carbon Dioxide Capture from Large Anthropogenic Point Sources". In: *ChemSusChem* 2.9 (2009), pp. 796–854. DOI: 10.1002/cssc.200900036.

[15] A Dąbrowski. "Adsorption — from theory to practice". In: *Advances in Colloid and Interface Science* 93.1-3 (2001), pp. 135–224. DOI: 10.1016/S0001-8686(00)00082-8.

[16] B. C. Camacho, R. P. Ribeiro, I. a.a.C. Esteves, and J. P. Mota. "Adsorption equilibrium of carbon dioxide and nitrogen on the MIL-53(Al) metal organic framework". In: *Separation and Purification Technology* 141 (2015), pp. 150–159. DOI: 10.1016/j.seppur.2014.11.040.

[17] J. Liu, P. K. Thallapally, B. P. McGrail, D. R. Brown, and J. Liu. "Progress in adsorption-based CO 2 capture by metal–organic frameworks". In: *Chem. Soc. Rev.* 41.6 (2012), pp. 2308–2322. ISSN: 0306-0012. DOI: 10.1039/C1CS15221A.

[18] D. Bazer-Bachi, L. Assié, V. Lecocq, B. Harbuzaru, and V. Falk. "Towards industrial use of metal-organic framework: Impact of shaping on the MOF properties". In: *Powder Technology* 255 (2014), pp. 52–59. DOI: 10.1016/j.powtec.2013.09.013.

[19] R. J. Kuppler, D. J. Timmons, Q.-R. Fang, J.-R. Li, T. a. Makal, M. D. Young, D. Yuan, D. Zhao, W. Zhuang, and H.-C. Zhou. "Potential applications of metal-organic frameworks". In: *Coordination Chemistry Reviews* 253.23-24 (2009), pp. 3042–3066. ISSN: 00108545. DOI: 10.1016/j.ccr.2009.05.019.

[20] P. Mishra, H. P. Uppara, B. Mandal, and S. Gumma. "Adsorption and Separation of Carbon Dioxide Using MIL-53(Al) Metal-Organic Framework". In: *Industrial & Engineering Chemistry Research* 53.51 (2014), pp. 19747–19753. ISSN: 0888-5885. DOI: 10.1021/ie5006146.

[21] W. Y. Hong, S. P. Perera, and A. D. Burrows. "Manufacturing of metal-organic framework monoliths and their application in CO2 adsorption". In: *Microporous and Mesoporous Materials* 214 (2015), pp. 149–155. ISSN: 13871811. DOI: 10.1016/j.micromeso.2015.05.014.

[22] A. I. Spjelkavik, Aarti, S. Divekar, T. Didriksen, and R. Blom. "Forming MOFs into Spheres by Use of Molecular Gastronomy Methods". In: *Chemistry - A European Journal* 20.29 (2014), n/a–n/a. ISSN: 09476539. DOI: 10.1002/chem.201402464.

[23] F. Akhtar, L. Andersson, S. Ogunwumi, N. Hedin, and L. Bergström. "Structuring adsorbents and catalysts by processing of porous powders". In: *Journal of the European Ceramic Society* 34.7 (2014), pp. 1643–1666. DOI: 10.1016/j.jeurceramsoc.2014.01.008.

[24] F. Rezaei, M. a. Sakwa-Novak, S. Bali, D. M. Duncanson, and C. W. Jones. "Shaping amine-based solid CO2 adsorbents: Effects of pelletization pressure on the physical and chemical properties". In: *Microporous and Mesoporous Materials* 204 (2015), pp. 34–42. ISSN: 13871811. DOI: 10.1016/j.micromeso.2014.10.047.

[25] V. Finsy, L. Ma, L. Alaerts, D. De Vos, G. Baron, and J. Denayer. "Separation of CO2/CH4 mixtures with the MIL-53(Al) metal–organic framework". In: *Microporous and Mesoporous Materials* 120.3 (2009), pp. 221–227. ISSN: 13871811. DOI: 10.1016/j.micromeso.2008.11.007.

[26] F. Rouquerol, J. Rouquerol, and K. Sing. *Adsorption by Powders & Porous Solids: Principles, Methodology and Applications*. Marseille: Academic Press, 1999. ISBN: 0-12-598920-2.

[27] B. K. Dutta. "Principles of mass transfer and separation processes". In: *The Canadian Journal of Chemical Engineering* 87.5 (2009), pp. 818–819. DOI: 10.1002/cjce.20228.

[28] J.-r. Li, J. Sculley, and H.-c. Zhou. "Metal–Organic Frameworks for Separations". In: *Chemical Reviews* 112.2 (2012), pp. 869–932. ISSN: 0009-2665. DOI: 10.1021/cr200190s.

[29] P. C. Wankat. *Separation Process Engineering: Includes Mass Transfer Analysis*. 3rd. Prentice Hall, 2012. ISBN: 978-0-13-138227-5.

[30] J. D. Seader, E. J. Henley, and D. K. Roper. *Separation Process Principles: Chemical and Biochemical Operations*. 3rd. John Wiley & Sons, Inc., 2011. ISBN: 978-0-470-48183-7.

[31] J. Keller and R. Staudt. *Gas adsorption equilibria - Experimental methods and adsorption isotherms*. New York: Springer, 2005, p. 442. ISBN: 0-387-23597-3. URL: http://www.tandfonline.com/doi/abs/10.1080/03602548408058530.

[32] J.-G. Choi, D. D. Do, and H. D. Do. "Surface Diffusion of Adsorbed Molecules in Porous Media: Monolayer, Multilayer, and Capillary Condensation Regimes". In: *Industrial & Engineering Chemistry Research* 40.19 (2001), pp. 4005–4031. DOI: 10.1021/ie010195z.

[33] M. Thommes, K. Kaneko, A. V. Neimark, J. P. Olivier, F. Rodriguez-Reinoso, J. Rouquerol, and K. S. Sing. "Physisorption of gases, with special reference to the evaluation of surface area and pore size distribution (IUPAC Technical Report)". In: *Pure and Applied Chemistry* 87.9-10 (2015), pp. 1051–1069. ISSN: 1365-3075. DOI: 10.1515/pac-2014-1117.

[34] R. T. Yang. *Adsorbents: Fundamentals and Applications*. Vol. 30. 1. New Jersey: John Wiley & Sons, Inc., 2003, pp. 117–157. ISBN: 0-471-29741-0.

[35] B. YILMAZ, N. TRUKHAN, and U. MÜLLER. "Industrial Outlook on Zeolites and Metal Organic Frameworks". In: *Chinese Journal of Catalysis* 33.1 (2012), pp. 3–10. DOI: 10.1016/S1872-2067(10)60302-6.

[36] D. D. Do. *Adsorption Analysis: Equilibria and Kinetics*. Vol. 2. Series on Chemical Engineering Imperial College Press. London: Imperial College Press, 1998, p. 913. DOI: 10.1142/9781860943829.

[37] J. L. Rowsell and O. M. Yaghi. "Metal–organic frameworks: a new class of porous materials". In: *Microporous and Mesoporous Materials* 73.1-2 (2004), pp. 3–14. ISSN: 13871811. DOI: 10.1016/j.micromeso.2004.03.034.

[38] P. Silva, S. M. F. Vilela, J. P. C. Tomé, and F. A. Almeida Paz. "Multifunctional metal–organic frameworks: from academia to industrial applications". In: *Chem. Soc. Rev.* 44.19 (2015), pp. 6774–6803. DOI: 10.1039/C5CS00307E.

[39] R. Ben-Mansour, M. Habib, O. Bamidele, M. Basha, N. Qasem, A. Peedikakkal, T. Laoui, and M. Ali. "Carbon capture by physical adsorption: Materials, experimental investigations and numerical modeling and simulations – A review". In: *Applied Energy* 161 (2016), pp. 225–255. DOI: 10.1016/j.apenergy.2015.10.011.

[40] P. G. Yot, Z. Boudene, J. Macia, D. Granier, L. Vanduyfhuys, T. Verstraelen, V. Van Speybroeck, T. Devic, C. Serre, G. Férey, N. Stock, and G. Maurin. "Metal–organic frameworks as potential shock absorbers: the case of the highly flexible MIL-53(Al)". In: *Chem. Commun.* 50.67 (2014), pp. 9462–9464. ISSN: 1359-7345. DOI: 10.1039/C4CC03853C.

[41] M. I. Nandasiri, S. R. Jambovane, B. P. McGrail, H. T. Schaef, and S. K. Nune. "Adsorption, separation, and catalytic properties of densified metal-organic frameworks". In: *Coordination Chemistry Reviews* 311 (2016), pp. 38–52. ISSN: 00108545. DOI: 10.1016/j.ccr.2015.12.004. URL: http://linkinghub.elsevier.com/retrieve/pii/S0010854515300655.

[42] G. Férey, C. Mellot-Draznieks, C. Serre, and F. Millange. "Crystallized Frameworks with Giant Pores: Are There Limits to the Possible?" In: *Accounts of Chemical Research* 38.4 (2005), pp. 217–225. ISSN: 0001-4842. DOI: 10.1021/ar040163i.

[43] K. Li, D. H. Olson, J. Y. Lee, W. Bi, K. Wu, T. Yuen, Q. Xu, and J. Li. "Multifunctional Microporous MOFs Exhibiting Gas/Hydrocarbon Adsorption Selectivity, Separation Capability and Three-Dimensional Magnetic Ordering". In: *Advanced Functional Materials* 18.15 (2008), pp. 2205–2214. ISSN: 1616301X. DOI: 10.1002/adfm.200800058.

[44] A. Lyubchyk, I. A. A. C. Esteves, F. J. A. L. Cruz, and J. P. B. Mota. "Experimental and Theoretical Studies of Supercritical Methane Adsorption in the MIL-53(Al) Metal Organic Framework". In: *The Journal of Physical Chemistry C* 115.42 (2011), pp. 20628–20638. DOI: 10.1021/jp207326d.

[45] A. Boutin, F.-X. Coudert, M.-A. Springuel-Huet, A. V. Neimark, G. Ferey, and A. H. Fuchs. "The Behavior of Flexible MIL-53(Al) upon CH 4 and CO 2 Adsorption". In: *The Journal of Physical Chemistry C* 114.50 (2010), pp. 22237–22244. DOI: 10.1021/jp10871 0h.

[46] C. Janiak and J. K. Vieth. "MOFs, MILs and more: concepts, properties and applications for porous coordination networks (PCNs)". In: *New Journal of Chemistry* 34.11 (2010), p. 2366. ISSN: 1144-0546. DOI: 10.1039/c0nj00275e.

[47] A. V. Neimark, F.-X. Coudert, C. Triguero, A. Boutin, A. H. Fuchs, I. Beurroies, and R. Denoyel. "Structural Transitions in MIL-53 (Cr): View from Outside and Inside". In: *Langmuir* 27.8 (2011), pp. 4734–4741. ISSN: 0743-7463. DOI: 10.1021/la200094x.

[48] A. Boutin, M.-A. Springuel-Huet, A. Nossov, A. Gédéon, T. Loiseau, C. Volkringer, G. Férey, F.-X. Coudert, and A. H. Fuchs. "Breathing Transitions in MIL-53(Al) Metal-Organic Framework Upon Xenon Adsorption". In: *Angewandte Chemie International Edition* 48.44 (2009), pp. 8314–8317. DOI: 10.1002/anie.200903153.

[49] F.-X. Coudert, A. Boutin, and A. H. Fuchs. "A thermodynamic description of the adsorption-induced structural transitions in flexible MIL-53 metal-organic framework". In: *Molecular Physics* 112.9-10 (2014), pp. 1257–1261. DOI: 10.1080/00268976.2014.889325.

[50] P. L. Llewellyn, G. Maurin, T. Devic, S. Loera-Serna, N. Rosenbach, C. Serre, S. Bourrelly, P. Horcajada, Y. Filinchuk, and G. Ferey. "Prediction of the Conditions for Breathing of Metal Organic Framework Materials Using a Combination of X-ray Powder Diffraction, Microcalorimetry, and Molecular Simulation". In: *Journal of the American Chemical Society* 130.38 (2008), pp. 12808–12814. ISSN: 0002-7863. DOI: 10.1021/ja803899q.

[51] E. Deniz, F. Karadas, H. A. Patel, S. Aparicio, C. T. Yavuz, and M. Atilhan. "A combined computational and experimental study of high pressure and supercritical CO2 adsorption on Basolite MOFs". In: *Microporous and Mesoporous Materials* 175 (2013), pp. 34–42. DOI: 10.1016/j.micromeso.2013.03.015.

[52] P. Mishra, S. Edubilli, H. P. Uppara, B. Mandal, and S. Gumma. "Effect of Adsorbent History on Adsorption Characteristics of MIL-53(Al) Metal Organic Framework". In: *Langmuir* 29.39 (2013), pp. 12162–12167. DOI: 10.1021/la4027128.

[53] J. Möllmer, M. Lange, A. Möller, C. Patzschke, K. Stein, D. Lässig, J. Lincke, R. Gläser, H. Krautscheid, and R. Staudt. "Pure and mixed gas adsorption of CH4 and N2 on the metal–organic framework Basolite® A100 and a novel copper-based 1,2,4-triazolyl isophthalate MOF". In: *Journal of Materials Chemistry* 22.20 (2012), p. 10274. ISSN: 0959-9428. DOI: 10.1039/c2jm15734a.

[54] A. F. Ferreira, A. M. Ribeiro, S. Kulaç, and A. E. Rodrigues. "Methane purification by adsorptive processes on MIL-53(Al)". In: *Chemical Engineering Science* 124 (2015), pp. 79–95. ISSN: 00092509. DOI: 10.1016/j.ces.2014.06.014.

[55] M. JACOBY. "HEADING TO MARKET WITH MOFS". In: *Chemical & Engineering News* 86.34 (2008), pp. 13–16. DOI: 10.1021/cen-v086n034.p013.

[56] M. Tagliabue, C. Rizzo, R. Millini, P. D. C. Dietzel, R. Blom, and S. Zanardi. "Methane storage on CPO-27-Ni pellets". In: *Journal of Porous Materials* 18.3 (2011), pp. 289–296. ISSN: 1380-2224. DOI: 10.1007/s10934-010-9378-0.

[57] G. W. Peterson, J. B. DeCoste, T. G. Glover, Y. Huang, H. Jasuja, and K. S. Walton. "Effects of pelletization pressure on the physical and chemical properties of the metal–organic frameworks Cu3(BTC)2 and UiO-66". In: *Microporous and Mesoporous Materials* 179 (2013), pp. 48–53. DOI: 10.1016/j.micromeso.2013.02.025.

[58] J. Freiding, F.-C. Patcas, and B. Kraushaar-Czarnetzki. "Extrusion of zeolites: Properties of catalysts with a novel aluminium phosphate sintermatrix". In: *Applied Catalysis A: General* 328.2 (2007), pp. 210–218. DOI: 10.1016/j.apcata.2007.06.017.

[59] C. A. Grande, V. I. Águeda, A. Spjelkavik, and R. Blom. "An efficient recipe for formulation of metal-organic Frameworks". In: *Chemical Engineering Science* 124 (2015), pp. 154–158. DOI: 10.1016/j.ces.2014.06.048.

[60] M. Rahman, A. Ahuja, S Baboota, B. S. P. Bhavna, V. Bali, N. Saigal, and J. Ali. "Recent Advances in Pelletization Technique for Oral Drug Delivery: A Review". In: *Current Drug Delivery* 6.1 (2009), pp. 122–129. ISSN: 15672018. DOI: 10.2174/156720109787048339.

[61] U. Meyer, A. Larsson, H.-P. Hentze, and R. Caruso. "Templating of Porous Polymeric Beads to Form Porous Silica and Titania Spheres". In: *Advanced Materials* 14.23 (2002), pp. 1768–1772. DOI: 10.1002/1521-4095(20021203)14:23<1768::AID-ADMA1768>3.0.CO;2-0.

[62] D. Bazer-Bachi, L. Assié, V. Lecocq, B. Harbuzaru, and V. Falk. "Towards industrial use of metal-organic framework: Impact of shaping on the MOF properties". In: *Powder Technology* 255 (2014), pp. 52–59. ISSN: 00325910. DOI: 10.1016/j.powtec.2013.09.013.

[63] J. Kim, S.-H. Kim, S.-T. Yang, and W.-S. Ahn. "Bench-scale preparation of Cu3(BTC)2 by ethanol reflux: Synthesis optimization and adsorption/catalytic applications". In: *Microporous and Mesoporous Materials* 161 (2012), pp. 48–55. DOI: 10.1016/j.micromeso.2012.05.021.

[64] D. Serrano, R. Sanz, P. Pizarro, I. Moreno, P. de Frutos, and S. Blázquez. "Preparation of extruded catalysts based on TS-1 zeolite for their application in propylene epoxidation". In: *Catalysis Today* 143.1-2 (2009), pp. 151–157. DOI: 10.1016/j.cattod.2008.09.039.

[65] J. Ren, N. M. Musyoka, H. W. Langmi, A. Swartbooi, B. C. North, and M. Mathe. "A more efficient way to shape metal-organic framework (MOF) powder materials for hydrogen storage applications". In: *International Journal of Hydrogen Energy* 40.13 (2015), pp. 4617–4622. DOI: 10.1016/j.ijhydene.2015.02.011.

[66] T. K. Bose, R. Chahine, and J.-M. St-Arnaud. *High-Density Adsorbent and Method of Producing Same*. 1991.

[67] R. P. P. L. Ribeiro, R. J. S. Silva, I. a. a. C. Esteves, and J. P. B. Mota. "Development, Construction, and Operation of a Multisample Volumetric Apparatus for the Study of Gas Adsorption Equilibrium". In: *Journal of Chemical Education* 92.4 (2015), pp. 757–761. ISSN: 0021-9584. DOI: 10.1021/ed500633h.

[68] Sigma-Aldrich. *Aluminum terephthalate, Basolite® A100 produced by BASF*. 2015. URL: http://www.sigmaaldrich.com/catalog/product/aldrich/688738 (visited on 10/30/2015).

[69] *Guide for the Use of the International System of Units (SI)*. 2008th ed. Washington, D.C.: U.S. Government Printing Office, 1995.

[70] I. Silverson Machines. *Preparation of Polyvinyl Alcohol (PVA) Solutions*. Tech. rep. 62CAI. East Longmeadow, MA, p. 4. URL: http://www.silverson.com/images/uploads/documents/CPVASolutions.pdf.

[71] Sigma-Aldrich. *Poly(vinyl alcohol), MOWIOL® 10-98*. 2006. URL: http://www.sigmaaldrich.com/catalog/product/aldrich/10852 (visited on 10/01/2015).

[72] Y. Ishii, Y. Nishiwaki, A. Al-zubaidi, and S. Kawasaki. "Pore Size Determination in Ordered Mesoporous Materials Using Powder X-ray Diffraction". In: *The Journal of Physical Chemistry C* 117.35 (2013), pp. 18120–18130. DOI: 10.1021/jp4057362.

[73] A. J. P. Setim. "Upgrade of an Experimental Volumetric Unit for Gas Adsorption Equilibrium Studies". MSc. Dissertation. Caparica: Faculdade de Ciências e Tecnologias da Universidade Nova de Lisboa, 2014, p. 54.

[74] E. Lemmon, M. McLinden, and D. Friend. "Thermophysical Properties of Fluid Systems". In: *NIST Chemistry WebBook, NIST Standard Reference Database Number 69*. Ed. by P. L. Mallard and W.G. Gaithersburg MD: National Institute of Satandards and Technology. URL: http://webbook.nist.gov/chemistry/fluid/.

[75] A. U. Garate. "Adsorbent Particle Design for Application in Gas Adsorption Processes". Errasmus Project. Caparica: Faculdade de Ciências e Tecnologias da Universidade Nova de Lisboa, 2016, pp. 1–55.

[76] A. Altomare, C. Cuocci, C. Giacovazzo, A. Moliterni, R. Rizzi, N. Corriero, and A. Falcicchio. *EXPO2014*. Bari, 2013. URL: http://www.ba.ic.cnr.it/content/expo.

[77] T. Loiseau, C. Serre, C. Huguenard, G. Fink, F. Taulelle, M. Henry, T. Bataille, and G. Férey. "A Rationale for the Large Breathing of the Porous Aluminum Terephthalate (MIL-53) Upon Hydration". In: *Chemistry - A European Journal* 10.6 (2004), pp. 1373–1382. ISSN: 0947-6539. DOI: 10.1002/chem.200305413.

[78] Y. Liu, J.-H. Her, A. Dailly, A. J. Ramirez-Cuesta, D. A. Neumann, and C. M. Brown. "Reversible Structural Transition in MIL-53 with Large Temperature Hysteresis". In: *Journal of the American Chemical Society* 130.35 (2008), pp. 11813–11818. ISSN: 0002-7863. DOI: 10.1021/ja803669w.

Appendix

A.1 Drop Test Results

Table A.1 shows the results of the drop tests performed on the samples containing binder along with the calculated average and associated error. The error was calculated using the standard deviation equation A.1.

$$\sigma_x = \sqrt{\frac{1}{n-1}\sum_{i=1}^{n}(x_i - \bar{x})^2} \tag{A.1}$$

Table A.1: Results of the drop tests on the samples containing binder: Batch B1 (2% PVA binder), Batch B1 (5% PVA binder), Batch B1 (10% PVA binder) and Batch B7 (15% PVA binder)

Sample	Batch B1	Batch B3	Batch B5	Batch B7
1	4	8	8	>30
2	5	4	5	>30
3	5	4	7	>30
4	5	5	8	>30
5	4	3	12	>30
6	6	5	9	n/a
7	7	4	3	n/a
8	1	4	6	n/a
9	2	9	6	n/a
10	5	5	8	n/a
11	2	3	9	n/a
12	3	4	8	n/a
13	5	8	8	n/a
14	6	7	7	n/a
15	2	6	5	n/a
16	1	4	8	n/a
17	2	7	6	n/a
18	1	6	10	n/a
19	6	6	7	n/a
20	3	8	8	n/a
Average	**3.75**	**5.50**	**7.4**	**>30**
Error	**1.92**	**1.82**	**1.96**	**n/a**

A.2 X-Ray Diffraction (XRD) Results

Figures A.1, A.2 and A.3 show experimental XRD patterns of MIL-53(Al) powder and binderless samples A1 compressed at 1tf and A2 compressed at 0.5tf and their most predominant peaks. Table A.2 shows the crystallographic unit cell parameters obtained for MIL-53(Al) powder using the software Expo2014.

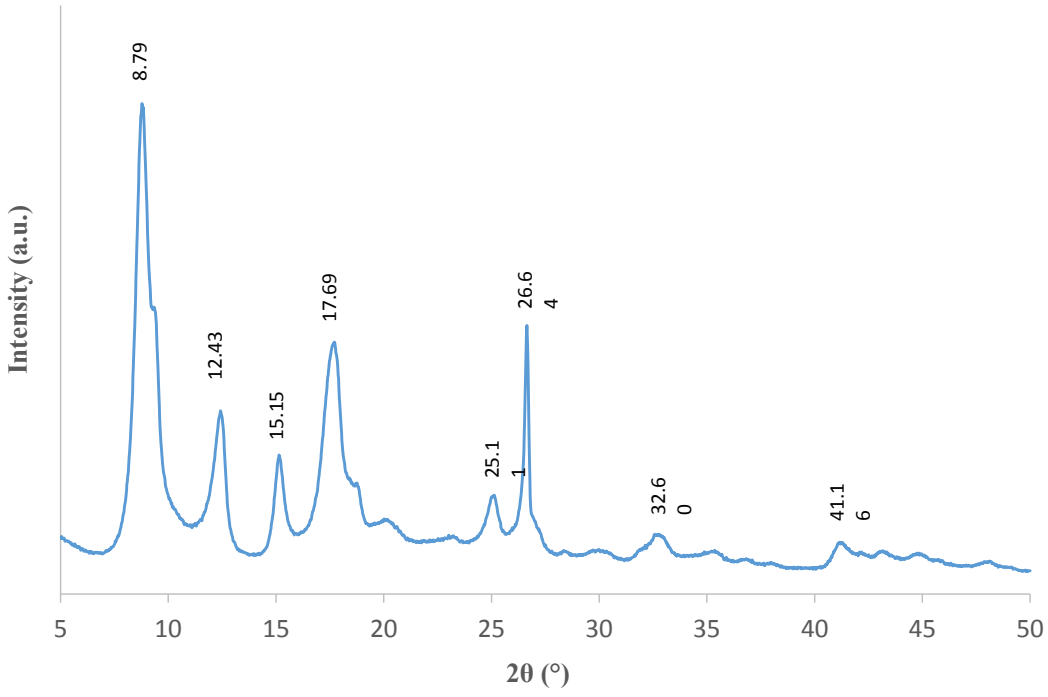

Figure A.1: Experimental XRD pattern of MIL-53(Al) powder.

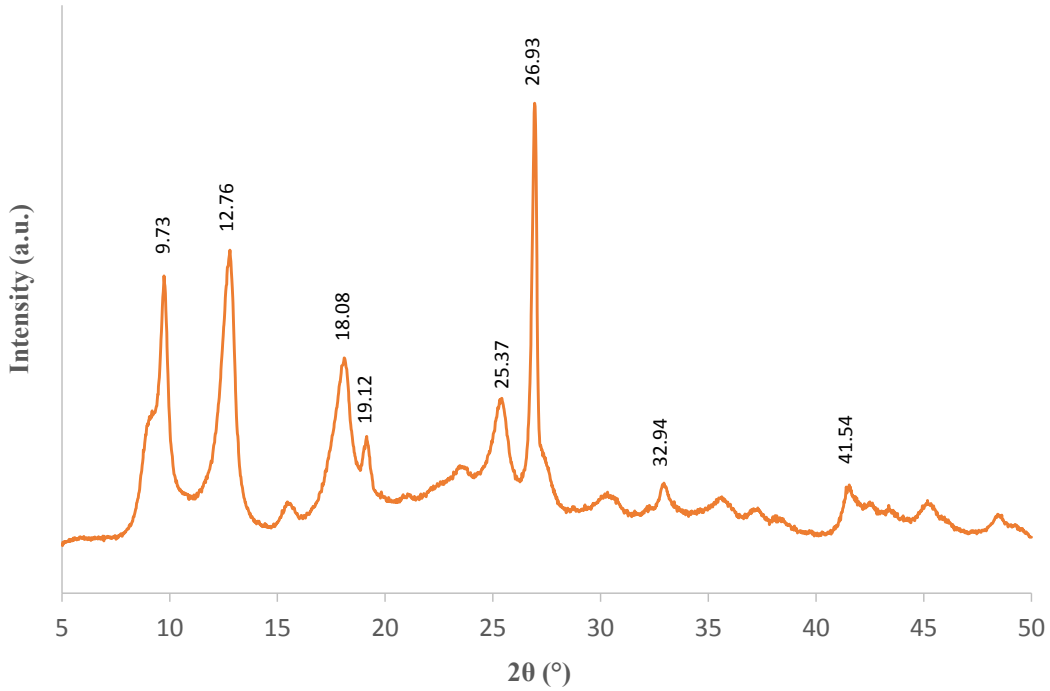

Figure A.2: Experimental XRD pattern of sample A1 compressed at 1tf.

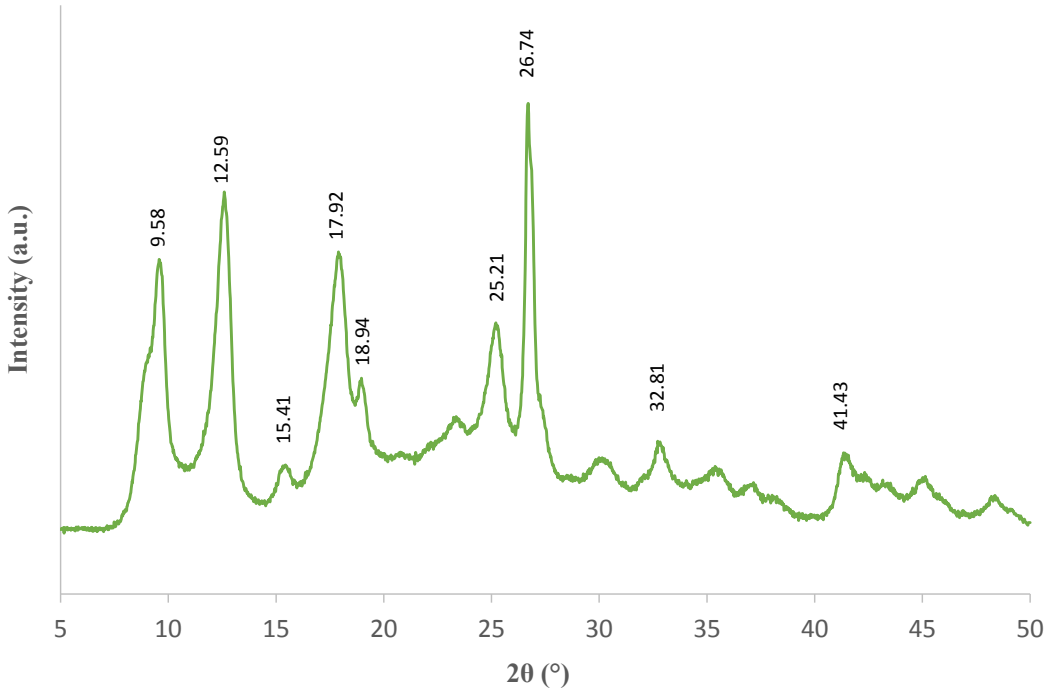

Figure A.3: Experimental XRD pattern of sample A1 compressed at 0.5tf.

Table A.2: Crystallographic unit cell parameters obtained for MIL-53(Al) powder.

Formula	$Al(OH)[O_2C\text{-}C_6H_4\text{-}CO_2].H_2O$
Crystal System	CC
Space Group	CC
a (Å)	20.401
a (Å)	7.677
a (Å)	6.888
$\alpha(°)$	90.00
$\beta(°)$	103.86
$\gamma(°)$	90.00
Volume Å	1047.28

A.3 Thermogravimetric Analysis (TGA) Results

Figures A.4, A.5, A.6 and A.7 show the TGA results for the samples containing binder. Figures A.8, A.9, A.10, A.11 and A.12 show the TGA results of the tests performed at a constant temperature for the samples containing binder and also for the PVA sample.

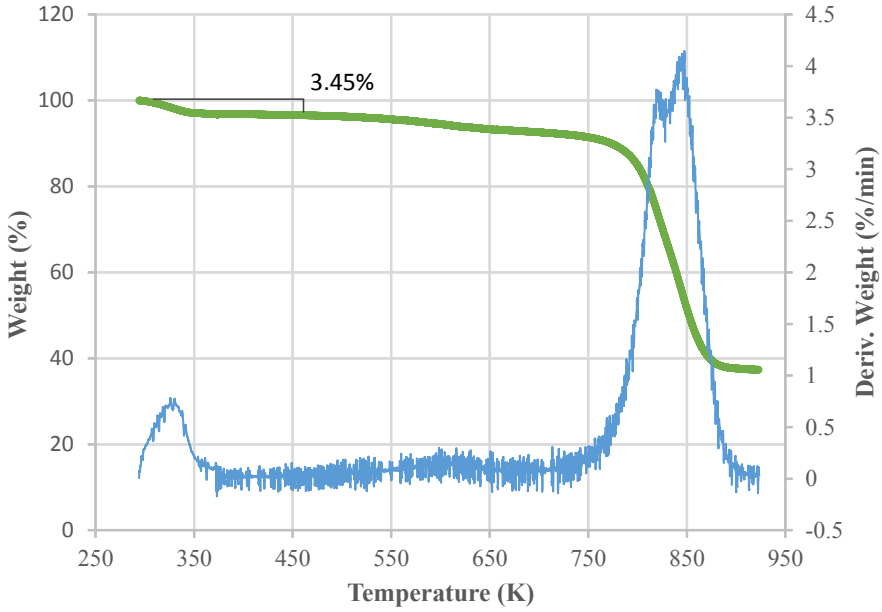

Figure A.4: TGA of sample B1 with 2% PVA binder.

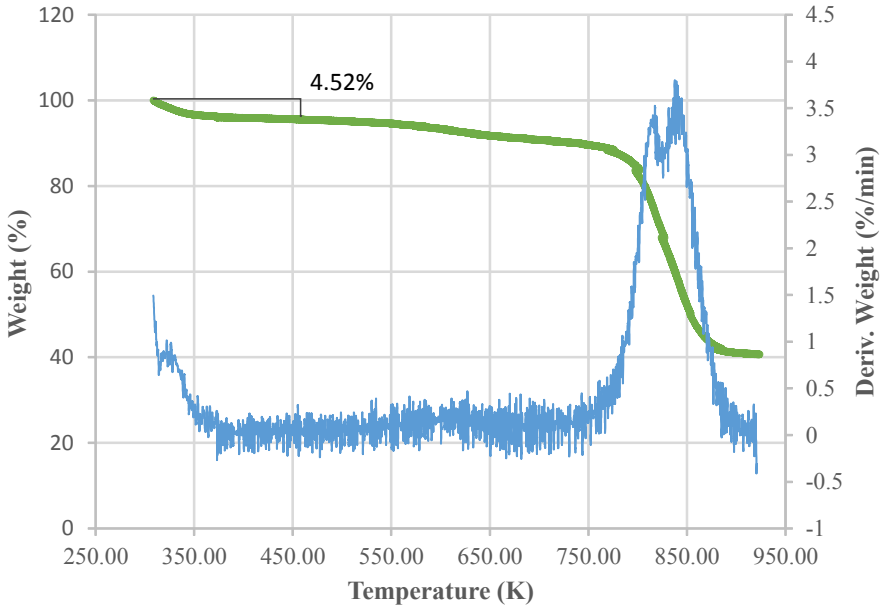

Figure A.5: TGA of sample B3 with 5% PVA binder.

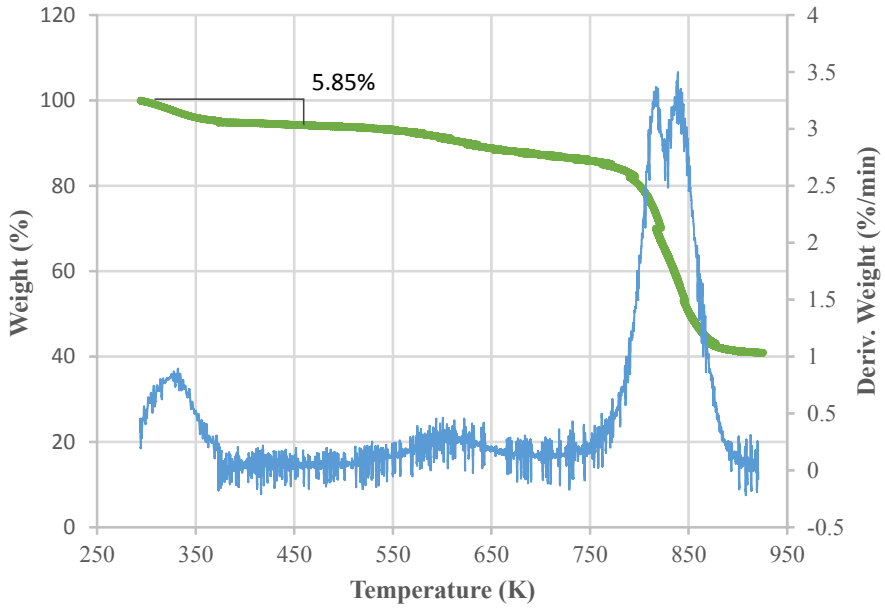

Figure A.6: TGA of sample B5 with 10% PVA binder.

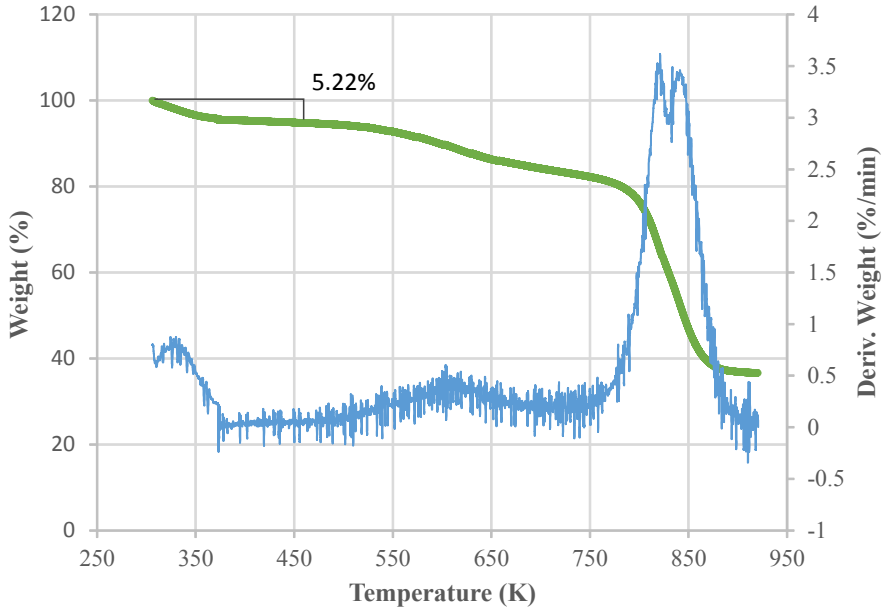

Figure A.7: TGA of sample B1 with 15% PVA binder.

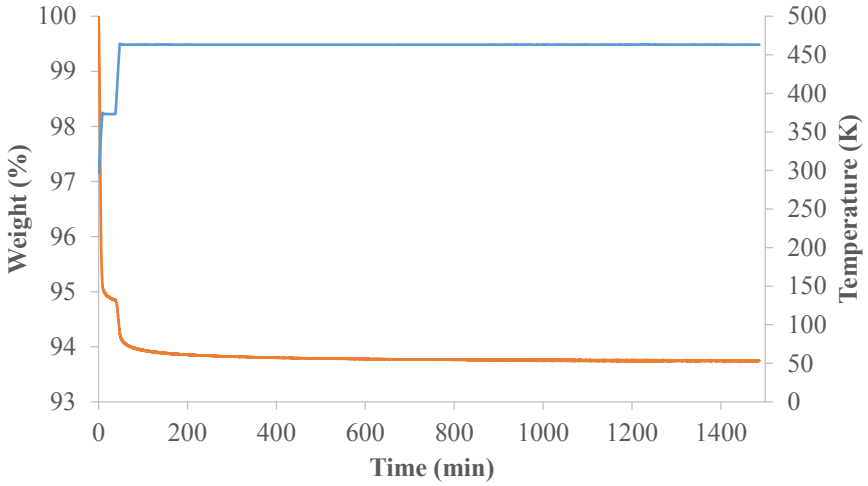

Figure A.8: TGA of sample B1 with 2% PVA binder at a 473K constant temperature.

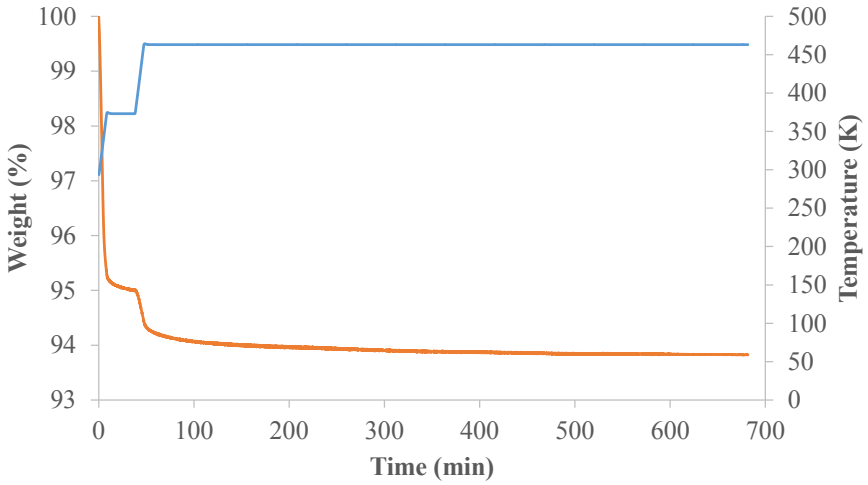

Figure A.9: TGA of sample B3 with 5% PVA binder at a 473K constant temperature.

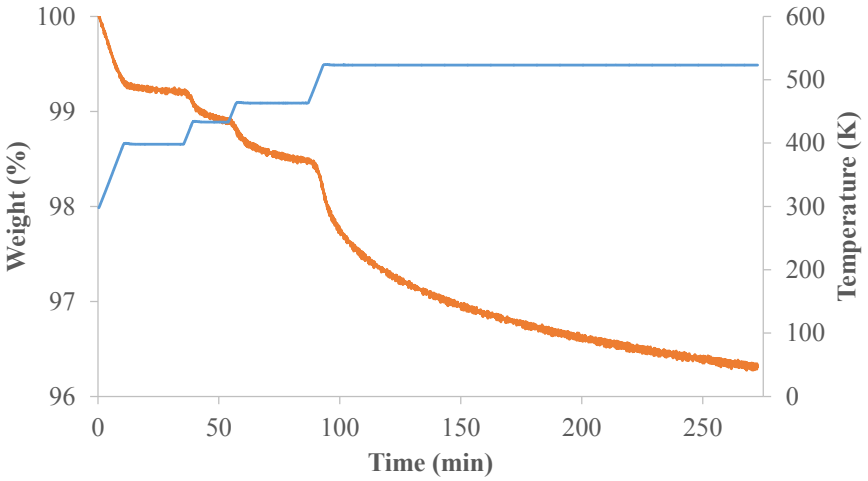

Figure A.10: TGA of sample B5 with 10% PVA binder at a 473K constant temperature.

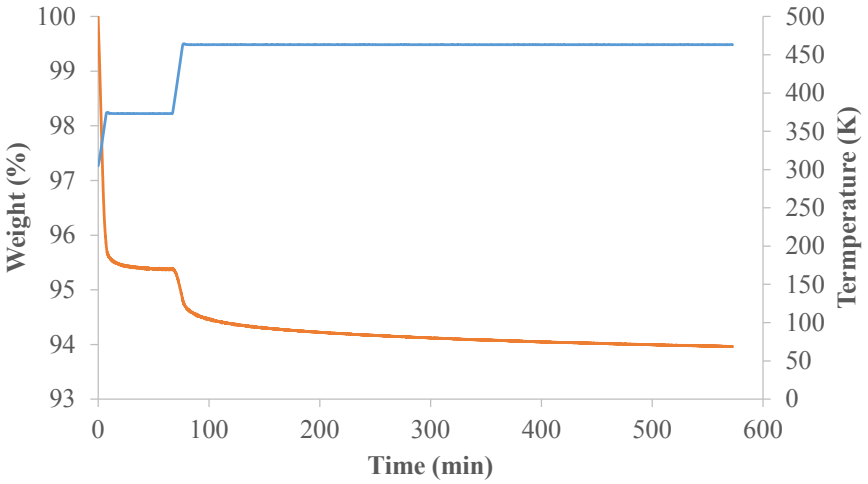

Figure A.11: TGA of sample B7 with 15% PVA binder at a 473K constant temperature.

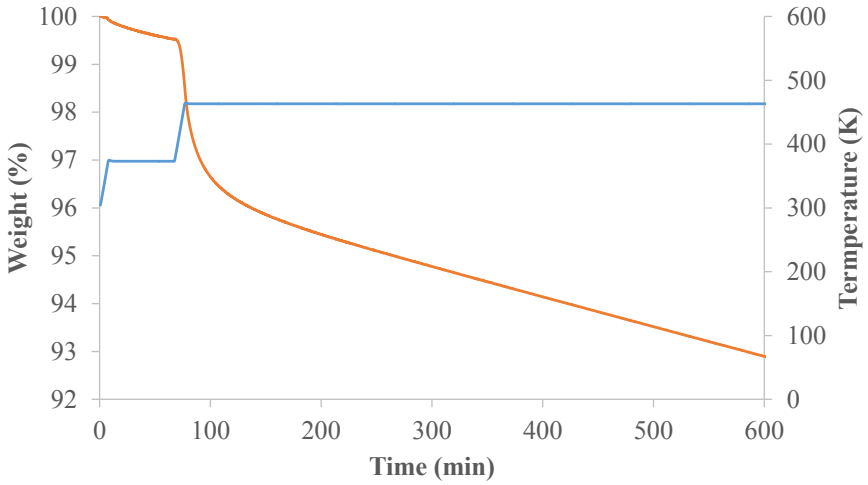

Figure A.12: TGA of pure PVA (Mowiol® 10-98) at a 473K constant temperature.

A.4 Calibration of the volumetric unit

This calibration refers to the volumetric unit shown in Figure 3.10. In order to simplify only the calibration of $Vcell_1$ will be described, since the calibration of $Vcell_2$ is identical. The calibration of these volumes were obtained by using helium (He) gas provided by Praxair (Portugal) with a purity of 99.999%. During the whole usage of this unit valves V0, V5 and V8 were always maintained closed, while valves V3 and V7 were always open. All the densities obtained in this section were retrieved from the NIST Standard Reference Database [74].

- **Step 1,** the first step to calibrate the cell volumes ($Vcel_1$ and $Vcel_2$) is to depressurize and evacuate the whole line using the vacuum pump with only valves V2, V4, V6, V9 and V10 open. Once the line is depressurized V10 is closed.

- **Step 2,** the second step is to release He into the unit up to by opening valve V1, with V2, V4, V6 and V9. Once the pressure desired is achieved (approximately 1atm), V2 and V9 is closed. This pressure is maintained and registered with aid of the pressure transducers (PT_1 and PT_2) and the in-house software for approximately 10 minutes and and average pressure is obtained. The temperatures shown in TI_1 and TI_1 are also registered. These first pressure will be denoted as initial pressures (P_i) and the initial temperatures (T_i). Knowing these two parameters it is possible to know the initial densities (ρ_{i}).

- **Step 3,** the third step is to first close valve V4 and V9 and then open V2 and V6. Afterward valve V1 is open until pressure rises significantly. Valve 2 and 6 are then once more closed and the pressure in Vref is maintained for approximately 10 minutes. The reference pressures (P_{ref}) and the reference temperatures (T_{ref}) are registered so the reference densities (ρ_{ref}) can be obtained.

- **Step 4,** the last step is the expansion of Vref to Vcell. This expansion is achieved by opening V4 and V9. This expansion is registered and maintained for at least 10 minutes. The final pressures (P_f) and the final temperatures (T_f) are registered so the final densities (ρ_{f}) can be obtained.

This process is repeated 5 times in order to calculate an average volume for the cells and their associated error. The experimental results obtained to calculate the volumes are shown in Tables A.3A.4. To calculate each experimental cell volume a modification of the ideal gas law was used (Equations A.2 and A.3) and is shown in Tabel A.5 along with the calculated average and associated error. The error was calculated using the standard deviation equation (Equation A.4).

$$PV = nRT \tag{A.2}$$

Table A.3: Experimental results for the calibration of $Vcell_1$.

Exp	P_i (bar)	T_i (°C)	ρ_i (kg/m^3)	P_{ref} (bar)	T_{ref} (°C)	ρ_{ref} (kg/m^3)	P_f (bar)	T_f (°C)	ρ_f (kg/m^3)
1	1.063	24.5	0.172	4.861	24.5	0.784	4.361	24.6	0.704
2	1.054	24.4	0.170	6.453	24.7	1.040	5.745	25.1	0.925
3	1.053	25.0	0.170	7.137	24.9	1.149	6.336	24.9	1.020
4	1.061	24.9	0.1710	10.268	24.9	1.651	9.050	25.0	1.455
5	1.086	25.0	0.175	11.213	25.0	1.801	9.871	25.0	1.587

Table A.4: Experimental results for the calibration of the volume $Vcell_2$.

Exp	P_i (bar)	T_i (°C)	ρ_i (kg/m^3)	P_{ref} (bar)	T_{ref} (°C)	ρ_{ref} (kg/m^3)	P_f (bar)	T_f (°C)	ρ_f (kg/m^3)
1	1.045	26.0	0.168	4.851	26.0	0.779	4.338	26.1	0.697
2	1.031	26.0	0.168	6.454	25.6	1.037	5.718	25.5	0.919
3	1.026	24.5	0.166	7.134	24.5	1.150	6.307	24.4	1.018
4	1.036	24.4	0.167	10.274	24.4	1.652	9.014	24.4	1.452
5	1.060	24.4	0.171	11.220	24.4	1.803	9.837	24.4	1.584

$$Vcell = \frac{\rho_{ref} Vref - \rho_f Vref}{\rho_f - \rho_i} \tag{A.3}$$

Table A.5: Calculated results of the cell volumes using equation A.3.

Exp	$Vcell_1$ (cm^3)	$Vcell_2$ (cm^3)
1	6.3095	6.4750
2	6.3551	6.4994
3	6.2770	6.4636
4	6.3256	6.4352
5	6.3189	6.4226
Average (cm^3)	**6.32**	**6.46**
Error	**0.03**	**0.03**

$$\sigma_x = \sqrt{\frac{1}{n-1}\sum_{i=1}^{n}(x_i - \bar{x})^2} \tag{A.4}$$

A.5 Adsorption Equilibria Measurements

The adsorption equilibria measurements were carried out in the volumetric unit shown in Figure 3.10. Each sample was tested in either one of the unit cells (Cell 1 or Cell 2) and the quantities of adsorbent were previously weighed. Before proceeding with the measurements the adsorbents were degassed. To degas the samples they were heated at a rate of 2°C/min up to 200°C or 190°C for the binderless samples or for the samples

with binder respectively and maintained at these temperatures for 3 hours under vacuum. Afterwards the temperature during the measurements was maintained at 30ºC in the oven and this temperature is considered the temperature that is in the cells (T_{cell1} and T_{cell2}). Before proceeding with the equilibria measurements, leaks were once more checked by using Helium (He) since it is an inert gas. Helium (He) used was provided by Praxair (Portugal) with a purity of 99.999%. For the adsorption equilibrium measurements the adsorbate used was carbon dioxide (CO_2)provided by Air Liquid (Portugal) with a purity of 99.998%. All the densities obtained were retrieved from the NIST Standard Reference Database [74].

- **Step 1,** the first step is to add the desired pressure to the reference volumes (V_{ref1} and V_{ref2}), with V4 and V9 closed and V1, V2 and V6 open. Once the pressure and temperature stabilizes the initial reference pressures ($P_{Vref1,i}$ and $P_{Vref2,i}$) and the initial reference temperatures ($T_{Vref1,i}$ $T_{Vref2,i}$) are registered in order to obtain the initial densities in the reference volumes($\rho_{ref1,i}$ and $\rho_{ref2,i}$.

- **Step 2,** the gas that was contained in V_{ref1} and V_{ref2} is then expanded into the cell that contains the adsorbent (V_{cell1} and V_{cell2}) by opening V4 and V9. The pressure is now monitored until the adsorption equilibrium is reached. In order to determine if equilibrium is reached, it is assumed that equilibrium is achieved once the rate change of the pressure approaches zero under isothermal conditions, in this case when the variation on the pressure is lower than 0.01 bar (witch is the accuracy of the pressure transducer used in the unit) [67]. Once equilibrium is reached the final total pressures ($P_{VTotal1,f}$ and $P_{VTotal2,f}$) and the final temperatures in the reference volumes (($T_{Vref1,f}$ $T_{Vref2,f}$)) are registered so the final densities in the reference volumes and the cell volumes ($\rho_{ref1,f}$, $\rho_{ref2,f}$ and $\rho_{cell1,f}$ and $_{cell2,f}$) can be obtained.

- **Step 3,** V4 and V9 are closed once again and Step 1 and Step 2 are repeated another 7 times.

- **Step 4,** after 8 points of adsorption are retreived an additional 5 points of dessorption are obtained. For the dessorption points the method is identical but in reverse. With valves V4 and V9 closed valves V2 and V6 are opened and now the pressure is decreased by opening V11 (or V10 if vacuum pressure is desired).

A maximum total of 13 points are retrieved by this method. The experimental results obtained to calculate the adsorption equilibrium and respective graphical representation are shown in section A.6.

The quantities of each sample that were packed in each cell are shown in Table A.6. In some cases due to gas leaks in the system a second run was performed. The mass loss in for the binderless samples were assumed to be the same as for the powder, while for the samples with binder the mass loss was retrieved from the TGA results. The experimental

results of each adsorption and desorption equilibria are presented in table A.7 to table A.15.

Table A.6: Samples Packed in the Volumetric Unit

Sample	Run	Cell	Mass Packed (g)	Mass Loss (%)	Final Mass (g)
A1	1	$Cell_1$	1.5501	2.00	1.5191
A2	1	$Cell_2$	1.3475	2.00	1.3206
A2	2	$Cell_1$	1.2424	2.00	1.2176
B1	1	$Cell_1$	0.9245	3.45	0.8931
B3	1	$Cell_2$	0.8875	4.52	0.8479
B3	2	$Cell_2$	0.6113	4.52	0.5837
B5	1	$Cell_1$	0.7097	5.85	0.6682
B7	1	$Cell_2$	0.9058	5.22	0.8585
B7	2	$Cell_1$	0.6125	5.22	0.5805

A.6 Adsorption Equilibria Measurements Results

All of the experimental results obtained to calculate the CO_2 adsorption equilibria measurements at 30ºC are shown. Tables A.7 to A.15 show the experimental results obtained for all of the six samples analysed in this work along with the calculated calculate net amount adsorbed at equilibrium. Figures A.13 to A.18 show represent all of the CO_2 adsorption equilibrium isotherms (30ºC) for all of the six samples tested in this work

Table A.7: CO_2 adsorption equilibria measurements at 30ºC for sample A1 compressed at 1tf (Run 1).

Exp	$P_{Vref1,i}$ (bar)	$P_{Vtotal1,f}$ (bar)	$T_{Vref1,i}$ (K)	$T_{Vref1,f}$ (K)	$\rho_{Vref1,i}$ (g/cm^3)	$\rho_{Vref1,f}$ (g/cm^3)	$\rho_{Vcell1,f}$ (g/cm^3)	q_{net} (mol/kg)
0	0.047	0.047	295.05	295.05	0.000084	0.000084	0.000082	0.000
1	0.644	0.179	295.35	295.55	0.001158	0.000321	0.000313	0.498
2	1.696	0.925	295.75	295.75	0.003062	0.001663	0.001622	1.244
3	2.215	1.759	295.85	295.55	0.004009	0.003185	0.003097	1.616
4	3.305	2.869	295.25	294.85	0.006028	0.005228	0.005079	1.926
5	5.506	4.922	294.85	293.75	0.010179	0.009107	0.008801	2.240
6	8.655	8.044	293.65	295.35	0.016365	0.014910	0.014612	2.595
7	14.313	13.282	295.35	294.75	0.027806	0.025706	0.024810	2.936
8	19.053	18.396	294.65	296.75	0.038300	0.036447	0.035381	3.088
9	9.929	11.100	296.75	296.15	0.018680	0.021077	0.020490	3.006
10	5.013	6.052	296.15	296.85	0.009198	0.011130	0.010883	2.714
11	3.065	3.689	297.25	297.15	0.005544	0.006697	0.006556	2.406
12	0.885	1.653	297.35	296.95	0.001582	0.002971	0.002909	1.888
13	0.070	0.673	297.15	296.75	0.000125	0.001205	0.001179	1.381

Table A.8: CO_2 adsorption equilibria measurements at 30°C for sample A2 compressed at 0.5tf (Run 1).

Exp	$P_{Vref1,i}$ (bar)	$P_{Vtotal1,f}$ (bar)	$T_{Vref1,i}$ (K)	$T_{Vref1,f}$ (K)	$\rho_{Vref1,i}$ (g/cm^3)	$\rho_{Vref1,f}$ (g/cm^3)	$\rho_{Vcell1,f}$ (g/cm^3)	q_{net} (mol/kg)
0	0.009	0.009	294.45	294.45	0.000016	0.000016	0.000016	0.000
1	0.606	0.165	294.65	294.55	0.001092	0.000297	0.000288	0.538
2	1.662	0.943	294.85	294.95	0.003010	0.001701	0.001654	1.321
3	2.183	1.752	294.95	294.15	0.003961	0.003179	0.003097	1.719
4	3.275	2.839	294.25	293.85	0.005994	0.005191	0.005025	2.078

Table A.9: CO_2 adsorption equilibria measurements at 30°C for sample A2 compressed at 0.5tf (Run 2).

Exp	$P_{Vref1,i}$ (bar)	$P_{Vtotal1,f}$ (bar)	$T_{Vref1,i}$ (K)	$T_{Vref1,f}$ (K)	$\rho_{Vref1,i}$ (g/cm^3)	$\rho_{Vref1,f}$ (g/cm^3)	$\rho_{Vcell1,f}$ (g/cm^3)	q_{net} (mol/kg)
0	0.038	0.038	293.55	293.55	0.000069	0.000069	0.000066	0.000
1	6.472	4.154	293.55	292.65	0.012089	0.007684	0.007399	2.550
2	9.284	8.329	293.75	294.35	0.017613	0.015675	0.015152	3.138
3	15.239	14.144	293.95	293.05	0.029967	0.027730	0.026547	3.528
4	18.904	18.286	293.35	293.65	0.038205	0.036745	0.035147	3.645
5	9.521	10.792	293.35	293.65	0.018117	0.020667	0.019888	3.468
6	5.645	6.513	293.65	293.75	0.010491	0.012159	0.011739	3.136
7	3.117	3.837	293.95	293.25	0.005706	0.007070	0.006824	2.659
8	1.064	1.831	294.15	294.25	0.001925	0.003326	0.003225	1.998
9	0.054	0.724	294.45	293.95	0.000097	0.001309	0.001269	1.289

Table A.10: CO_2 adsorption equilibria measurements at 30°C for sample B1 containing 2% PVA binder (Run 1).

Exp	$P_{Vref1,i}$ (bar)	$P_{Vtotal1,f}$ (bar)	$T_{Vref1,i}$ (K)	$T_{Vref1,f}$ (K)	$\rho_{Vref1,i}$ (g/cm^3)	$\rho_{Vref1,f}$ (g/cm^3)	$\rho_{Vcell1,f}$ (g/cm^3)	q_{net} (mol/kg)
0	0.044	0.044	297.75	297.75	0.000078	0.000078	0.000077	0.000
1	0.551	0.246	297.85	296.15	0.000982	0.000440	0.000430	0.516
2	1.692	1.140	296.25	296.75	0.003049	0.002045	0.002001	1.324
3	2.251	1.928	296.75	295.45	0.004062	0.003489	0.003397	1.705
4	4.375	3.855	295.45	296.45	0.008020	0.007017	0.006857	2.210
5	7.565	6.880	296.35	296.95	0.014066	0.012715	0.012423	2.742
6	9.985	9.518	296.75	297.05	0.018792	0.017844	0.017423	2.940
7	14.622	13.912	297.15	297.05	0.028236	0.026761	0.026078	3.108
8	19.134	18.422	296.95	296.35	0.038056	0.036574	0.035437	3.169
9	15.654	16.065	296.85	297.95	0.030463	0.031188	0.030481	3.200
10	10.901	11.562	298.05	296.95	0.020515	0.021969	0.021396	3.124
11	4.588	5.703	296.95	297.25	0.008375	0.010445	0.010237	2.730
12	2.083	2.803	297.55	297.05	0.003745	0.005067	0.004960	2.181
13	0.053	0.817	297.25	293.45	0.000094	0.001480	0.001432	1.284

Table A.11: CO_2 adsorption equilibria measurements at 30°C for sample B3 containing 5% PVA binder (Run 1).

Exp	$P_{Vref1,i}$ (bar)	$P_{Vtotal1,f}$ (bar)	$T_{Vref1,i}$ (K)	$T_{Vref1,f}$ (K)	$\rho_{Vref1,i}$ (g/cm^3)	$\rho_{Vref1,f}$ (g/cm^3)	$\rho_{Vcell1,f}$ (g/cm^3)	q_{net} (mol/kg)
0	0.010	0.010	297.35	297.35	0.000018	0.000018	0.000017	0.000
1	0.520	0.236	297.45	295.65	0.000928	0.000423	0.000413	0.493
2	1.661	1.124	295.75	296.25	0.002998	0.002020	0.001973	1.311
3	2.220	1.880	296.45	294.85	0.004009	0.003408	0.003312	1.748
4	4.349	3.805	295.05	295.95	0.007983	0.006942	0.006766	2.309

Table A.12: CO_2 adsorption equilibria measurements at 30°C for sample B3 containing 5% PVA binder (Run 2).

Exp	$P_{Vref1,i}$ (bar)	$P_{Vtotal1,f}$ (bar)	$T_{Vref1,i}$ (K)	$T_{Vref1,f}$ (K)	$\rho_{Vref1,i}$ (g/cm^3)	$\rho_{Vref1,f}$ (g/cm^3)	$\rho_{Vcell1,f}$ (g/cm^3)	q_{net} (mol/kg)
0	0.016	0.016	293.35	293.35	0.000029	0.000029	0.000028	0.000
1	6.587	5.082	293.85	294.45	0.012298	0.009387	0.009094	2.424
2	8.594	8.003	293.95	293.05	0.016225	0.015111	0.014534	2.856
3	15.154	14.183	293.35	293.65	0.029864	0.027739	0.026626	3.249
4	19.055	18.412	293.55	293.65	0.038512	0.037030	0.035415	3.434
5	9.946	11.127	293.55	293.75	0.018958	0.021343	0.020543	3.320
6	5.269	6.151	293.95	293.15	0.009761	0.011499	0.011066	2.894
7	4.075	4.411	294.15	294.25	0.007494	0.008124	0.007867	2.681
8	1.516	2.072	294.45	293.85	0.002747	0.003773	0.003636	2.086
9	0.016	0.525	293.95	293.05	0.000029	0.000950	0.000919	1.280

Table A.13: CO_2 adsorption equilibria measurements at 30°C for sample B5 containing 10% PVA binder (Run 1).

Exp	$P_{Vref1,i}$ (bar)	$P_{Vtotal1,f}$ (bar)	$T_{Vref1,i}$ (K)	$T_{Vref1,f}$ (K)	$\rho_{Vref1,i}$ (g/cm^3)	$\rho_{Vref1,f}$ (g/cm^3)	$\rho_{Vcell1,f}$ (g/cm^3)	q_{net} (mol/kg)
0	0.055	0.055	291.85	291.85	0.000100	0.000100	0.000096	0.000
1	0.591	0.425	292.15	292.75	0.001074	0.000770	0.000744	0.290
2	1.249	0.983	292.85	291.85	0.002273	0.001792	0.001724	0.758
3	2.035	1.768	291.95	292.55	0.003730	0.003226	0.003113	1.172
4	3.842	3.403	293.15	292.55	0.007082	0.006271	0.006039	1.688
5	7.662	6.968	292.55	292.75	0.014466	0.013093	0.012588	2.220
6	9.822	9.424	292.95	293.25	0.018754	0.017929	0.017242	2.386
7	14.382	13.592	293.45	291.25	0.028189	0.026767	0.025433	2.634
8	19.308	18.642	291.35	291.85	0.039526	0.037642	0.035907	3.044
9	10.618	11.668	291.65	291.25	0.020482	0.022695	0.021604	2.992
10	4.225	5.340	291.15	291.65	0.007862	0.009982	0.009568	2.584
11	2.125	2.700	291.95	291.95	0.003897	0.004967	0.004775	2.103
12	0.970	1.365	291.75	291.35	0.001769	0.002498	0.002399	1.584
13	0.045	0.429	291.55	291.85	0.000082	0.000780	0.000751	0.952

Table A.14: CO_2 adsorption equilibria measurements at 30°C for sample B7 containing 15% PVA binder (Run 1).

Exp	$P_{Vref1,i}$ (bar)	$P_{Vtotal1,f}$ (bar)	$T_{Vref1,i}$ (K)	$T_{Vref1,f}$ (K)	$\rho_{Vref1,i}$ (g/cm^3)	$\rho_{Vref1,f}$ (g/cm^3)	$\rho_{Vcell1,f}$ (g/cm^3)	q_{net} (mol/kg)
0	0.024	0.024	291.85	291.85	0.000044	0.000044	0.000042	0.000
1	0.557	0.373	292.15	292.65	0.001074	0.000770	0.000744	0.265
2	1.214	0.919	292.65	291.75	0.002273	0.001792	0.001724	0.688
3	2.004	1.712	291.85	292.45	0.003730	0.003226	0.003113	1.054
4	3.818	3.341	293.15	292.35	0.007082	0.006271	0.006039	1.520
5	7.645	6.888	292.35	292.75	0.014466	0.013093	0.012588	2.064
6	9.810	9.366	292.95	293.25	0.018754	0.017929	0.017242	2.269

Table A.15: CO_2 adsorption equilibria measurements at 30°C for sample B7 containing 15% PVA binder (Run 2).

Exp	$P_{Vref1,i}$ (bar)	$P_{Vtotal1,f}$ (bar)	$T_{Vref1,i}$ (K)	$T_{Vref1,f}$ (K)	$\rho_{Vref1,i}$ (g/cm^3)	$\rho_{Vref1,f}$ (g/cm^3)	$\rho_{Vcell1,f}$ (g/cm^3)	q_{net} (mol/kg)
0	0.038	0.038	294.05	294.05	0.000068	0.000068	0.000066	0.000
1	8.150	6.590	294.35	294.55	0.015323	0.012271	0.011882	2.039
2	15.860	14.652	294.75	293.95	0.031199	0.028640	0.027579	2.317
3	19.055	18.514	294.65	294.85	0.038304	0.037045	0.035633	2.372
4	10.005	11.080	294.15	293.15	0.019031	0.021300	0.020451	2.438
5	2.946	4.137	293.25	293.45	0.005402	0.007630	0.007369	2.052
6	1.080	1.643	293.55	293.45	0.001959	0.002989	0.002891	1.483
7	0.045	0.450	293.35	293.15	0.000081	0.000814	0.000787	0.812

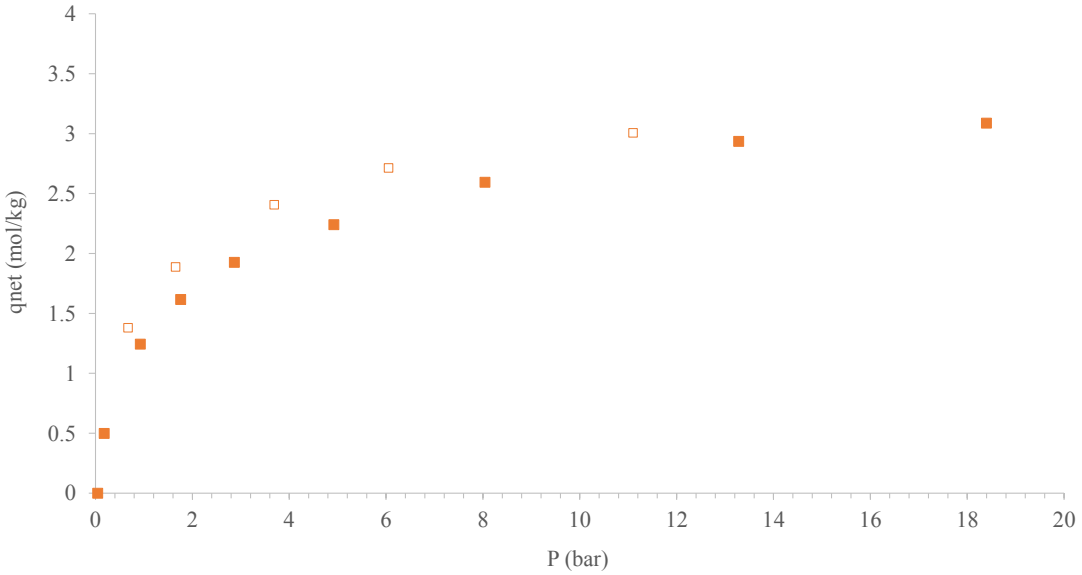

Figure A.13: Net adsorption equilibrium isotherms of CO_2 at 30°C on the sample A1 (binderless MIL-53(Al) pellets compressed at 1tf) Closed symbols denote adsorption data and open symbols denote desorption data.

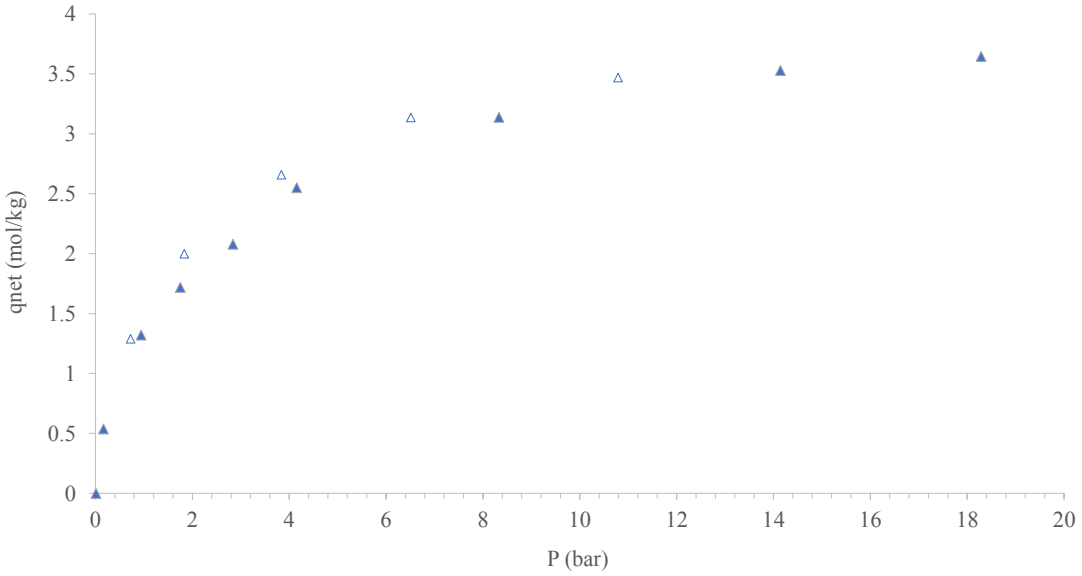

Figure A.14: Net adsorption equilibrium isotherms of CO_2 at 30°C on the sample A2 (binderless MIL-53(Al) pellets compressed at 0.5tf) Closed symbols denote adsorption data and open symbols denote desorption data.

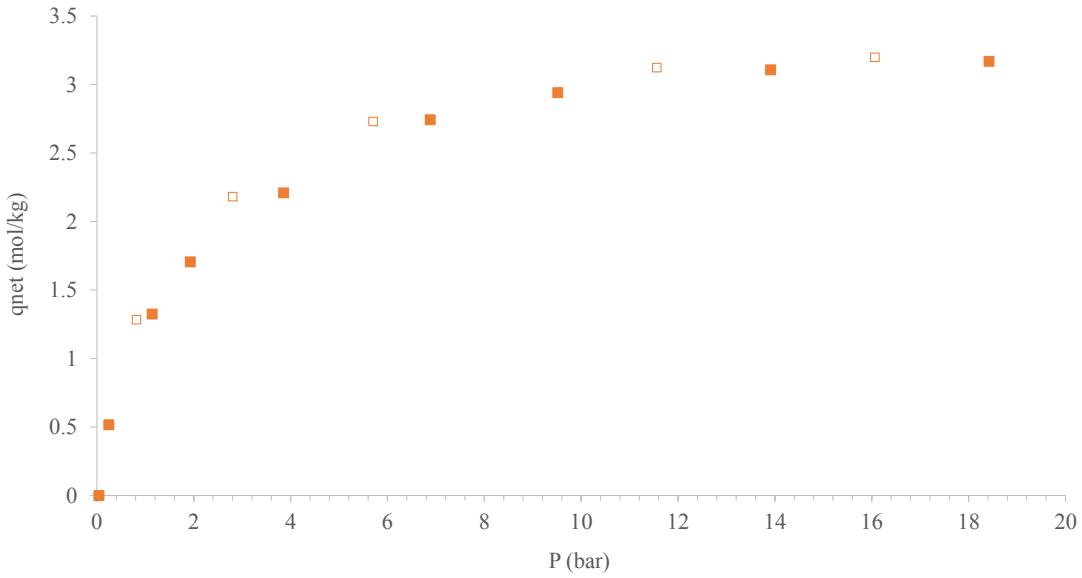

Figure A.15: Net adsorption equilibrium isotherms of CO_2 at 30ºC on the sample B1 (MIL-53(Al) with 2% PVA binder). Closed symbols denote adsorption data and open symbols denote desorption data.

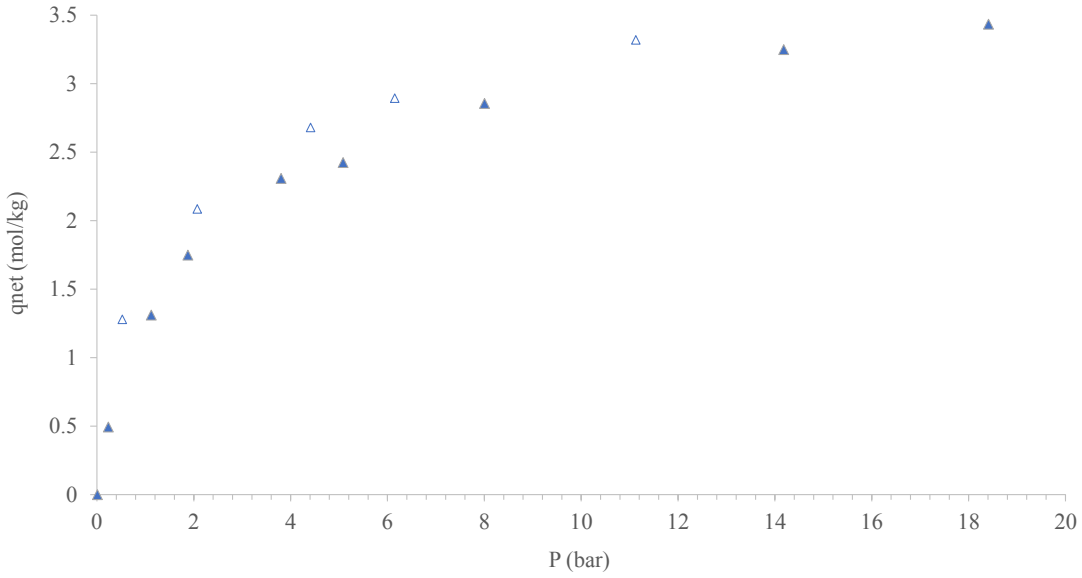

Figure A.16: Net adsorption equilibrium isotherms of CO_2 at 30ºC on the sample B3 (MIL-53(Al) with 5% PVA binder). Closed symbols denote adsorption data and open symbols denote desorption data.

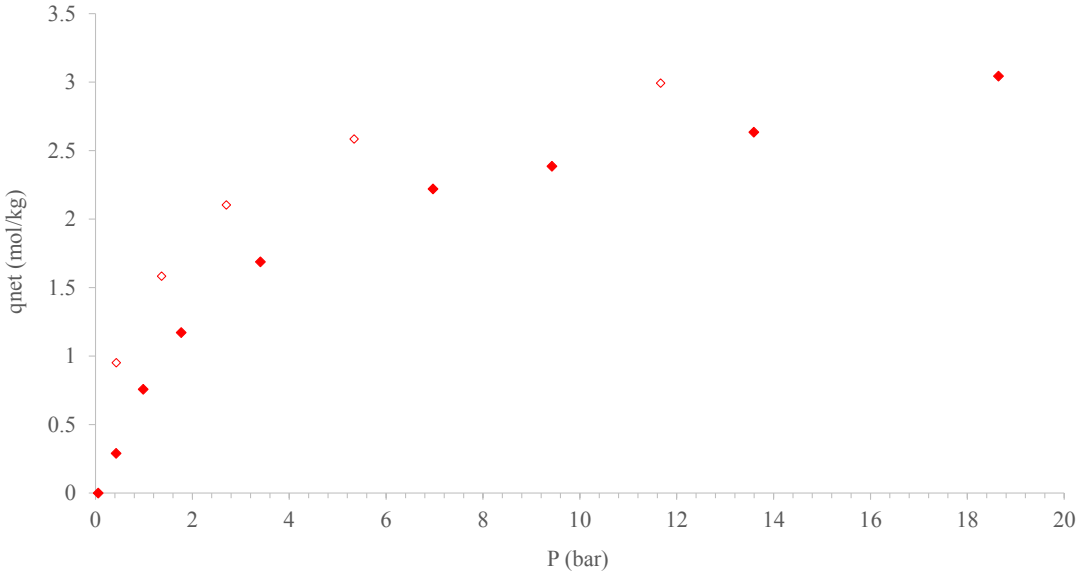

Figure A.17: Net adsorption equilibrium isotherms of CO_2 at 30ºC on the sample B5 (MIL-53(Al) with 10% PVA binder). Closed symbols denote adsorption data and open symbols denote desorption data.

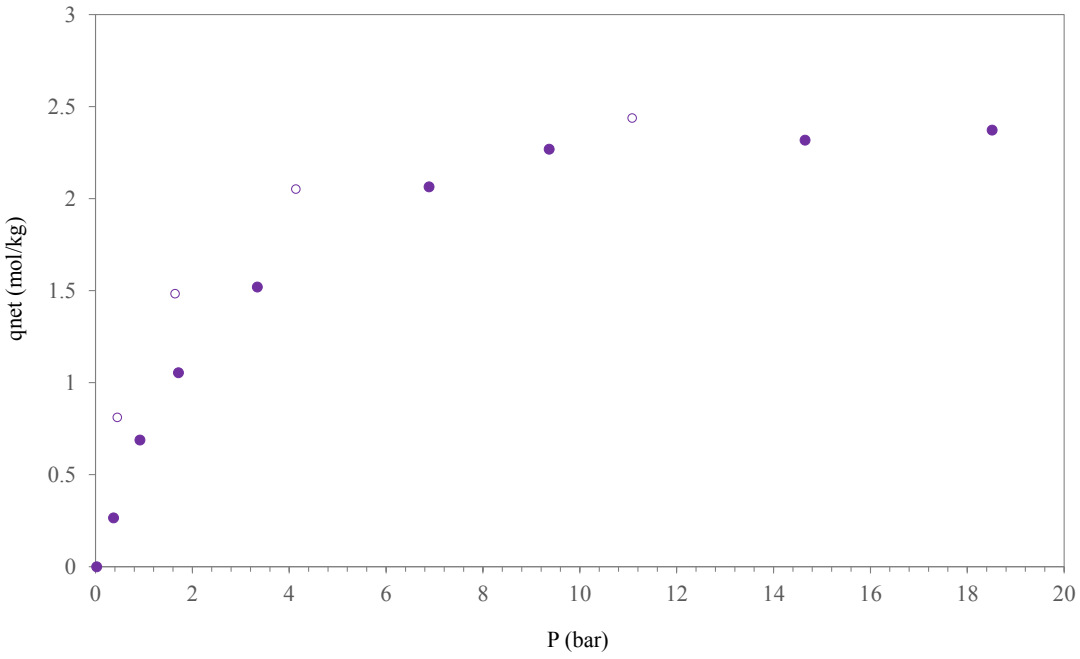

Figure A.18: Net adsorption equilibrium isotherms of CO_2 at 30ºC on the sample B7 (MIL-53(Al) with 15% PVA binder). Closed symbols denote adsorption data and open symbols denote desorption data.